AN ABSTRACT OF THE THESIS OF

Michael J. Ewald for the degree of Master of Science
in Marine Resource Management presented on November 18, 2013.

Title: Where's the Ground Surface? Elevation Bias in LIDAR-derived Digital Elevation Models Due to Dense Vegetation in Oregon Tidal Marshes

Abstract approved:

_____

Laura S. Brophy

Light Detection and Ranging (LIDAR) is a powerful resource for coastal and wetland managers and its use is increasing. Vegetation density and other land cover characteristics influence the accuracy of LIDAR-derived ground surface digital elevation models; however, the degree to which wetland land cover biases LIDAR estimates of the ground surface is largely unknown. The minimum-bin LIDAR gridding technique has been proposed as a way to mitigate dense vegetation interference to generate LIDAR-derived digital elevation models (DEM). Past research has focused on the ability to resolve the marsh plain elevation and only limited research has investigated the overall DEM accuracy across the landscape using a wide range of cell sizes and land cover classes.

I compared LIDAR-derived DEM accuracy across a 174 ha tidal wetland restoration site with a mix of native wetland and non-native agricultural pasture species. I found an optimum cell size of 1.4 m (1.96 m^2) with a mean positive bias of 4.5 cm and a mean absolute error of 24.3 cm. At cell sizes smaller than the optimum, vegetation interferes with the LIDAR sensor and positively biases DEM models. At cell sizes larger than 1.4 m, the DEM captures and favors low features within the

landscape, such as channels and ditches, which thereby degrade overall DEM performance.

In addition, I investigated LIDAR interference by twelve common tidal wetland vegetation associations across six Oregon estuaries, using survey-grade Global Positioning System (GPS) measurements of the wetland surface and quantitative vegetation data (percent cover by species) for each measurement location. The fundamental vertical accuracy (FVA) of the LIDAR datasets was 4.5 cm root mean square error (RMSE) and had no consistent positive or negative bias in open landcover. Within wetland vegetation communities, my results suggest that LIDAR estimates of the ground surface in tidal wetlands are typically 10 cm to 30 cm above GPS measurements. Plant associations dominated by *Carex obnupta* and *Carex lyngbyei* exhibited the largest discrepancy between LIDAR and GPS measurements (mean discrepancies 36.6 cm and 48.8 cm respectively). The smallest errors observed in the study were about 10 cm to 11 cm and occurred in several different plant associations, including two low tidal marsh associations dominated by a mixture of *Deschampsia cespitosa*, *Distichlis spicata*, *Sarcocornia perennis* and *Jaumea carnosa*.

These results suggest that the minimum-bin gridding technique for LIDAR may mitigate vegetation interference by densely vegetated land covers within LIDAR-derived DEM. However, care should be taken to select an appropriate cell size and validate the results before relying on the DEM for analysis. My research yields new information for coastal LIDAR users and increases our understanding of uncertainty in LIDAR-derived datasets to improve the ability to accurately evaluate and manage coastal environments.

Where's the Ground Surface? Elevation Bias in LIDAR-derived Digital Elevation Models Due to Dense Vegetation in Oregon Tidal Marshes

by
Michael J. Ewald

A THESIS

submitted to

Oregon State University

in partial fulfillment of
the requirements for the
degree of

Master of Science

Presented November 18, 2013
Commencement June 2014

Master of Science thesis of Michael J. Ewald presented on November 18, 2013.

APPROVED:

Major Professor, representing Marine Resource Management

Dean of the College of Earth, Ocean, and Atmospheric Sciences

Dean of the Graduate School

I understand that my thesis will become part of the permanent collection of Oregon State University libraries. My signature below authorizes release of my thesis to any reader upon request.

Michael J. Ewald, Author

ACKNOWLEDGEMENTS

The author expresses sincere appreciation to all those who contributed valuable support and insight throughout the completion of this research. Thank you, Laura Brophy, for your guidance and mentorship as the main advisor for my research. Thank you to my committee members Michael Olsen, Jim Graham, and Claudia Häse. Thank you to my colleagues and instructors in the Marine Resource Management Program and the College of Earth, Ocean, and Atmospheric Sciences for supporting my research and enhancing my education. Finally, thank you to all my friends and family for your support and encouragement.

TABLE OF CONTENTS

LIST OF FIGURES

LIST OF TABLES

LIST OF APPENDICES

LIST OF APPENDIX FIGURES

LIST OF APPENDIX TABLES

1 INTRODUCTION

The way we investigate and manage the environment and our existence within it is changing. Ecosystem Based Management (EBM) and Marine Spatial Planning (MSP) recognize that ecological, social, and environmental systems are linked, with complex relationships and feedbacks (Guichard and Peterson, 2009; McLeod and Leslie, 2009; Rosenberg and Sandifer, 2009). Managers are turning to EBM and MSP management approaches driven by scientific inquiry, analysis, and data to model environmental systems and assess impacts of management actions and other influences (Ricketts, 1992; Brock and Purkis, 2009). The shift to EBM and MSP is exciting and allows us to more effectively assess the outcome of management actions and describe environmental systems. Spatial modeling provides a key tool to EBM and often underlies key management decisions. As a result, understanding the strength and uncertainty of a chosen analysis path is critical to developing actionable information and environmental intelligence for management.

Uncertainty, if properly understood and communicated, does not lead to inadequate analysis or decisions, and managers must be comfortable making decisions under conditions of uncertainty (Rosenberg and Sandifer, 2009). However, the risk of faulty decision-making significantly increases if uncertainty around the inputs to analysis is unknown and managers require highly accurate and precise analysis. Uncertainty could be the result of the source data or gaps in knowledge of what would happen to an environmental or social system under a given set of conditions. In both cases, problems associated with the quality of the data can propagate and affect a manager's ability to make decisions, implement policies, or plan management interventions. If management action is taken based on faulty data, impacts may cascade to other sectors or lead to unexpected outcomes. EBM/MSP is capable of dealing with this uncertainty if the sources of uncertainty are known and

communicated throughout the management process (Ricketts, 1992; Brock and Purkis, 2009).

Geospatial analysis allows EBM/MSP frameworks to predict management outcomes across the landscape. Geospatial analysis is complex and typically blends many different data sources together into a final product. As a result, error in the source data and subsequent analysis is difficult to track and quantify. This, in turn, leads to incomplete understanding of the total error budget and how that translates to the products of analysis (Couclelis, 2003).

1.1 Introduction to LIDAR

Light Detection and Ranging (LIDAR) has emerged as a key tool for coastal EBM geospatial analysis because it is able to provide high spatial resolution, and highly accurate, elevation data compared to past digital elevation models such as the National Elevation Dataset (Brock and Purkis, 2009). LIDAR is a geospatial technology that uses a laser pulse to measure distance from the sensor to an object (Hodgson and Bresnahan, 2004; Wehr and Lohr, 1999). The sensor sends out tens to hundreds of thousands of laser pulses per second and accurately measures the time it takes for each pulse to travel from the sensor to the target, reflect off the target, and return to the sensor (Hodgson and Bresnahan, 2004; Wehr and Lohr, 1999). LIDAR sensors can be mounted to multiple platforms, including tripods (static), airplanes, helicopters, boats, and vehicles. Airborne platforms are the most common and the focus of this research.

In concept, LIDAR survey flights are very similar to cutting a lawn with a lawnmower (Figure 1.1). The LIDAR sensor has a field of view that the sensor is capable of measuring during each pass over the area of interest. The swath width is the horizontal extent, perpendicular to the flight path of a single flight line, that a LIDAR system is capable of scanning (Beraldin *et al.,* 2010). Swath width is a function of the field of view of the LIDAR sensor and the aircraft altitude above ground level (Beraldin *et al.,* 2010). Multiple flight lines may be required to cover an

area of interest on the landscape, just as it takes multiple cutting paths to fully trim the grass in a homeowner's lawn.

The particular LIDAR sensor, flight altitude, swath width, and many other parameters determine the LIDAR pulse return density and success of the system in mapping terrains (Hodgson and Bresnahan, 2004; Wehr and Lohr, 1999). Higher density measurements are more likely to accurately capture the structure of the landscape because more data is available for interpolation and processing. Each LIDAR laser pulse is georeferenced with high accuracy using survey grade inertial measurement units (IMU) and Global Positioning System (GPS) receivers, yielding a three-dimensional (3D) dataset consisting of billions of irregularly spaced points across the landscape. LIDAR point cloud data collected during the survey flight is not directly useful for most EBM/MSP geospatial analysis because the point cloud must first be processed into a gridded digital elevation model (DEM). DEM generation uses statistical methods to filter and interpolate the LIDAR point cloud, deriving a modeled ground surface elevation in a raster format that is compatible with common geospatial analysis techniques (Meng *et al.*, 2010). Gridded raster surfaces that represent the ground surface elevation at high spatial resolution provide an important base dataset to many environmental and ecological EBM/MSP studies that rely on geospatial data because many environmental and biological processes in coastal areas are tightly related to tidal inundation.

EBM/MSP approaches and associated analysis require this elevation data to accurately assess and model the relationships between different environmental and ecological concerns (Guichard and Peterson, 2009; McLeod and Leslie, 2009; Rosenberg and Sandifer, 2009). For example, LIDAR can be used to model the extent of tidal influence, map hydrologic restrictions and flow paths through the landscape, assess likely plant communities, model tsunami inundation impacts and evacuation routes, identify landslides, and many other tasks (Brock and Purkis, 2009).

In the context of tidal ecological research, LIDAR can be used as an important predictor of vegetation species presence and extent across the landscape (Moeslund *et*

al., 2011). Plant species presence within tidal wetlands is closely tied to the inundation frequency of tidal waters (Odum, 1985, 1988; Janousek and Folger, 2013; Cornu and Sadro, 2002). Elevation is a primary parameter of tidal inundation regimes because higher elevation areas of a tidal wetland are less likely to be flooded as the tidal waters rise and fall. As a result, elevation changes on the order of a few centimeters can lead to dramatic shifts in vegetation community structure (Janousek and Folger, 2013; Cornu and Sadro, 2002).

1.2 Motivation and Organization of This Thesis

Data accuracy and uncertainty in source data are critical challenges to EBM/MSP approaches that rely on comprehensive modeling and management strategies rooted in data. Understanding and communicating accuracy and uncertainty within DEM is critical to the success of inquiry and analysis of coastal ecosystems for both science and management purposes (Couclelis, 2003; Palmer, 2009; Simenstad *et al.,* 2005). If the error budget of input data to an EBM/MSP approach is unknown or incomplete, managers and others cannot effectively weigh the efficacy of a particular management strategy against other candidate strategies.

LIDAR data is heavily used within tidal wetland restoration and management at both site-specific and regional spatial scales. In these zones, environmental conditions and floristic development is often tightly linked to elevation (Cornu and Sadro, 2002; Brock and Purkis, 2009). These tight interactions require high resolution and accurate elevation data to accurately model and predict outcomes of management intervention (Palmer, 2009; Simenstad *et al.,* 2005; Cornu and Sadro, 2002; Kentula, 2000). Changes in elevation of a few centimeters can result in completely different vegetation communities and tidal hydrology (Odum, 1985, 1988; Janousek and Folger, 2013; Cornu and Sadro, 2002). The true outcome of a restoration project may significantly differ from the projected outcome if the underlying analysis used to design a project is based on inaccurate source elevation data (Palmer, 2009; Simenstad *et al.,* 2005; Cornu and Sadro, 2002; Kentula, 2000).

Vegetation planting plans, channel design, dike removal, and other restoration interventions are susceptible to inadequate accuracy in source elevation data. Restoration and management are necessary, but expensive. The best available science, analysis, and planning allow restoration and management projects to achieve the maximum ecological benefit while minimizing total cost.

LIDAR-derived DEMs are typically much more detailed than DEMs derived from photogrammetry, such as the National Elevation Dataset (NED). Increased spatial resolution and highly accurate reported fundamental vertical accuracy in open terrain can lead analysts and researchers into asking questions that require resolving minute differences in elevation across many different land cover classes and terrains. Unfortunately, the total LIDAR error budget may be larger than the maximum acceptable error for the types of analysis the data can support, especially in land cover classes that were not evaluated for LIDAR delivery quality assurance and validation.

For example, Ewald and Brophy (2012) delineated the area below highest measured tide (HMT) from a LIDAR-derived DEM for conservation and restoration planning purposes in the Tillamook Bay Estuary. The delineation of the HMT and other elevation-derived boundaries are sensitive to error in the DEM. Figure 1.2 maps HMT onto the flat (< 5 degree slope) landscape of the Tillamook Bay Estuary, Oregon. This example illustrates how sensitive DEM-based analysis can be, and has implications for the success of EBM/MSP approaches. The blue line in Figure 1.2 represents the best estimate of where HMT falls within the landscape. The zone within ± 0.5 m of the estimate is 174 m wide while the zone within ± 1.0 m is 374 m wide (Figure 1.2). This means that the blue line may fall anywhere within the 374 m wide strip around the estimate if the DEM has ± 1.0 m of error. The mapped elevation uncertainty bands in Figure 1.2 represent three common magnitudes of error in the DEM due to dense vegetation, as shown in Chapter 3. DEM uncertainty can have far-ranging and significant impacts in situations where the delineation of HMT or other boundaries directly influences management of the landscape.

The goal of my research is to narrow a data gap in LIDAR error estimates by adding data from tidal wetlands in the Pacific Northwest. The fundamental questions that link my research together are:

- Do tidal wetland vegetation communities interfere with LIDAR-derived estimates of the ground surface?
- If they do interfere, how does the magnitude of error differ across those land cover types? For example, does LIDAR error differ in *Carex obnupta* high marsh (Figures 1.3 and 1.4) vegetation communities versus low marsh environments (Figure 1.5)?
- Finally, can the effect of vegetation interference in LIDAR be mitigated using a simple minimum-bin filter DEM generation approach?

My research does not definitively resolve any of the questions that I have asked, but in combination with the work of other researchers, it helps build a clearer picture of an uncertain world.

This thesis is divided into four chapters plus appendices. Chapter One provides background information, an introduction to LIDAR and the organization of this thesis. Chapter Two assesses the effectiveness of the minimum-bin LIDAR filtering and gridding technique to mitigate the effect of vegetation in a LIDAR-derived DEM across a diked tidal wetland restoration site. Chapter Three investigates the role of twelve different vegetation communities common to Oregon tidal and coastal wetlands in LIDAR-derived DEM bias. Finally, Chapter Four concludes and summarizes the thesis. Six appendices accompany the main body of this thesis and provide definitions, diagnostic plots, summaries, and visualizations of the data and results.

1.3 Figures

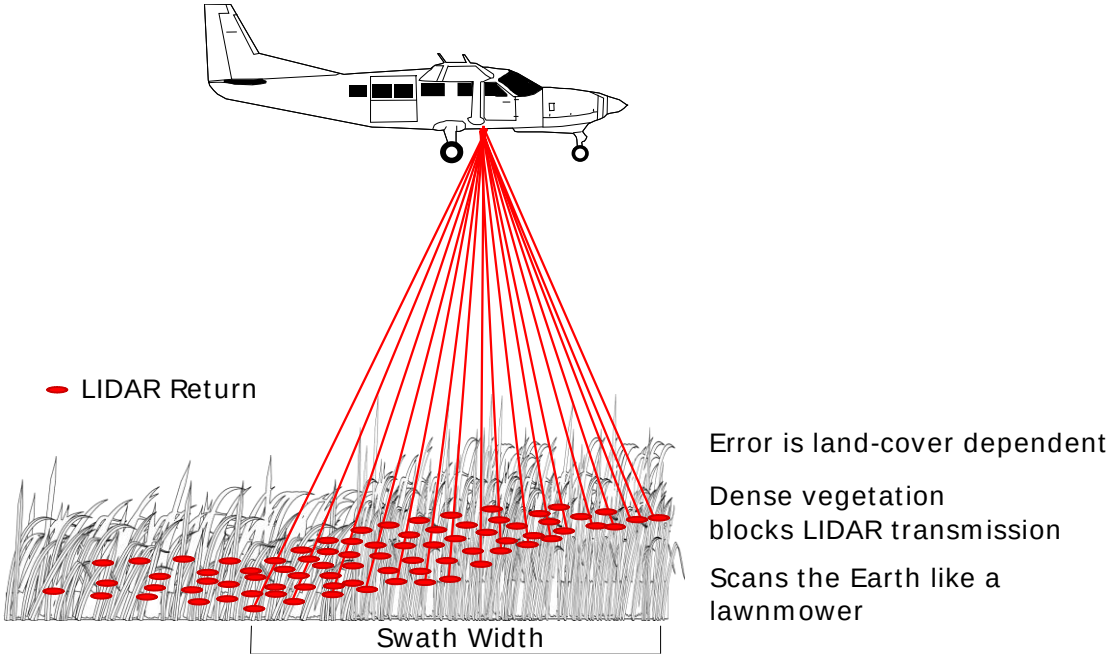

Figure 1.1: Airborne LIDAR scanning schematic. A LIDAR sensor is mounted on the aircraft where it scans the surface of the Earth with a lawnmower-like pattern, yielding a three-dimensional dataset consisting of LIDAR returns.

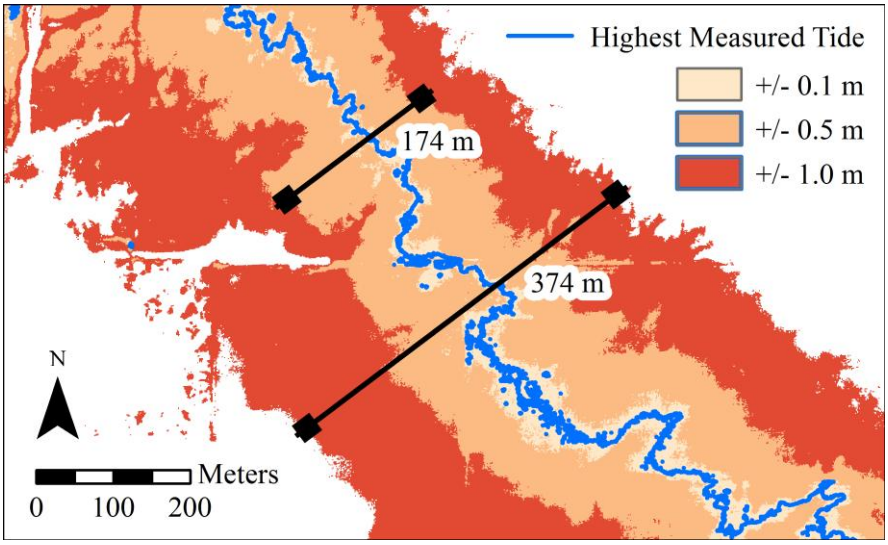

Figure 1.2: Illustration of DEM uncertainty. Highest measured tide (HMT) and three uncertainty bands are mapped onto the DEM in flat terrain.

Figure 1.3: Standing in a *Carex obnupta* wetland. In this figure, the 1.3 m (6 ft. 1in.) author is standing in a *Carex obnupta* (common name: slough sedge) tidal wetland. These wetlands are extremely difficult to work within and require "swimming" through the vegetation. Photo by Tammy Winfield.

Figure 1.4: Looking down in a *Carex obnupta* wetland. The ground surface is not visible when looking straight down (nadir) in a *Carex obnupta* wetland.

Figure 1.5: A typical low tidal marsh in the Siletz River Estuary, Oregon (USA). In this photo, wetland ecologist John Christy is estimating percent cover of vegetation species present within a one square meter quadrat along a survey transect. The same survey methods were used to collect much of the data analyzed in Chapter Three. Photo by Laura Brophy.

CHAPTER 2

LIDAR IN COASTAL WETLANDS: SELECTING THE OPTIMUM CELL SIZE FOR A MINIMUM-BIN DIGITAL ELEVATION MODEL

Michael J. Ewald

Marine Resource Management Program
Oregon State University

November 18, 2013

2 LIDAR IN COASTAL WETLANDS: SELECTING THE OPTIMUM CELL SIZE FOR A MINIMUM-BIN DIGITAL ELEVATION MODEL

2.1 Abstract

Light Detection and Ranging (LIDAR) is an important tool for environmental analysis, especially in coastal and estuarine systems. LIDAR-derived digital elevation model (DEM) estimates of the ground surface elevation are positively biased in densely vegetated environments, such as some emergent, shrub, and forested tidal wetlands. The minimum-bin gridding technique has been proposed as a way to mitigate the effect of dense vegetation in LIDAR-derived DEM. Past research has focused on the ability to resolve the marsh plain elevation and limited research has investigated the overall DEM accuracy across the landscape using a wide range of DEM raster cell sizes. The purpose of this study is to test LIDAR-derived DEM accuracy from cell sizes ranging from 0.1 m to 6.0 m (0.01 m^2 to 36.0 m^2) and select an optimum cell size for a 174 ha tidal wetland restoration site in the Coquille River Estuary, Oregon, USA. Vegetation associations at the site were dominated by a mix of native tidal wetland species and non-native agricultural pasture species. We found an optimum cell size of 1.4 m (1.96 m^2) with a mean positive bias of 4.5 cm and a mean absolute error of 24.3 cm. At cell sizes smaller than 1.4 m, dense vegetation interferes with the LIDAR sensor and positively biases DEM models. At cell sizes larger than 1.4 m, the DEM captures and favors low features within the landscape (e.g. channels) and degrades DEM performance. The results suggest that the minimum-bin gridding technique for LIDAR may mitigate vegetation interference within LIDAR-derived DEM; however, care should be taken to select an appropriate cell size and validate the results before relying on the DEM for analysis.

2.2 Introduction

Coastal environments contain important ecosystems with complex interactions and feedbacks, often tightly linked to elevation through the interface between rising and falling tidal water levels and the shoreline (Elliott and Whitfield, 2011). Complex spatial modeling, planning, and mapping technologies for coastal management are increasing in efforts to manage the environment holistically (Ricketts, 1992; Brock and Purkis, 2009). Managers are turning to models to identify the extent of tidal influence, to predict the effect of different sea-level rise scenarios, to map habitats, and many other tasks that have direct implications on coastal communities and ecosystems (e.g., Diefenderfer *et al.*, 2008; Poulter and Halpin, 2008; Schmid *et al*., 2011; Brock and Purkis, 2009; Chust *et al*., 2008; Lohani and Mason, 2001). Tidal wetlands are crucial landscapes nested within the coastal zone where elevation is a primary controlling factor in the development of vegetation, soil conditions, channel morphology, accretion, and other processes (Cornu and Sadro, 2002; Frenkel *et al.,* 1981). Therefore, management and restoration of these landscapes often require elevation information at both high spatial resolution and high elevation accuracy to properly assess and predict potential outcomes of management interventions (Athearn *et al.,* 2010). This is especially true in wetland restoration, where both passive and active approaches have been attempted with variable success (Palmer, 2009; Simenstad *et al.,* 2005; Cornu and Sadro, 2002; Kentula, 2000).

LIDAR (Light Detection And Ranging) is an emerging geospatial technology that is increasingly used by coastal and estuarine geospatial practitioners and scientists at both regional and site-specific spatial scales to provide high spatial resolution elevation data (Brock and Purkis, 2009). Airborne LIDAR uses a laser scanner mounted on an aircraft to scan the surface of the earth, much like a lawnmower (Wehr and Lohr, 1999). The particular LIDAR sensor, flight altitude, swath width, and many other parameters determine the LIDAR pulse return density and success of the system in mapping terrains (Hodgson and Bresnahan, 2004; Wehr and Lohr, 1999). Additionally, the filtering and interpolation techniques used to

transform as-received LIDAR point-cloud data to a raster-based digital elevation model (DEM) will affect the accuracy and efficacy of the model (Meng *et al.,* 2010; Bater and Coops, 2009; Wehr and Lohr, 1999).

Past research has shown that the estimated ground surface elevation derived from raster-based LIDAR-derived DEM are typically higher than surveyed elevations using survey-grade Global Positioning System (GPS) measurements of the tidal wetland ground surface (Schmid *et al.,* 2011; Chassereau *et al.,* 2011; Hladik and Alber, 2012; Athearn *et al.,* 2010; Wang *et al.,* 2009; Sadro *et al.,* 2007; Montané and Torres, 2006; Rosso *et al.,* 2006). These studies attribute the positive bias to dense wetland vegetation interfering with the LIDAR pulse and preventing it from reaching the true elevation of the marsh plain (Schmid *et al.,* 2011; Hladik and Alber, 2012; Sadro *et al.,* 2007). The separation of ground and vegetation in low-relief topography and short vegetation is challenging because statistical and morphological LIDAR classifiers typically look for large changes in slope and topographic shape, as well as shifts in surface elevation (Briese, 2010; Meng *et al.,* 2010).

LIDAR filters and classifiers are quite good at removing buildings and trees from a DEM where separation between ground and other landscape features is significant (Meng *et al.,* 2010). They are not as effective where a consistent patch of dense grass covers large regions of the area of interest or other even landcover where separation between ground points and features on the surface is minimal (Meng *et al.,* 2010). In addition, discrete return LIDAR systems are typically not able to discriminate vegetation canopy from ground because the half pulse length is longer than the vegetation is tall (Hladik and Alber, 2012). Therefore, LIDAR return filters and classifiers may identify the vegetation canopy as the ground instead of sparse points that better approximate the marsh plain.

Studies of LIDAR error have focused on *Spartina spp.* dominated tidal wetlands (Schmid *et al.,* 2011; Chassereau *et al.,* 2011; Hladik and Alber, 2012; Wang *et al.,* 2009). In these studies, the authors find that the mean

difference between LIDAR-derived elevations and GPS-surveyed elevations exhibit a positive bias of between 10 cm and 45 cm. Additionally, Montané and Torres (2006) found that topography within, and immediately surrounding, the LIDAR spot diameter did not significantly alter the results when comparing the difference between LIDAR-derived elevation and GPS-surveyed elevation in flat (i.e., < 10 degree slope) marsh topography. Hladik and Alber (2012) found that vegetation height was correlated with LIDAR error but that the difference between LIDAR-derived elevations and measured elevation was less than the total vegetation canopy height. Wang *et al*. (2009) found that LIDAR underestimated the canopy height of tidal wetland vegetation but that it was significantly correlated with leaves and other elements in the vegetation.

Multiple studies have attempted to compare interpolation and filtering techniques to produce DEMs that better approximate the marsh plain elevation of tidal wetlands (Montané and Torres, 2006; Wang *et al.*, 2009; Hladik and Alber, 2012). Hladik and Alber (2012) successfully developed correction factors for the main vegetation types within their study area using a field survey to map vegetation communities. Sadro *et al*. (2007) employed hyper-spectral remote sensing to map vegetation communities and developed species-specific correction factors. Their approach was successful but required significant ground control and advanced remote sensing to classify vegetation from remote data. As a result, the technical and analytical capabilities required to successfully mitigate vegetation interference of LIDAR may be difficult to apply for management purposes. Schmid *et al*. (2011) and Wang *et al*. (2009) employ a minimum-bin gridding technique to identify the optimum search radius for ground LIDAR returns and interpolate a raster DEM from the LIDAR point cloud. This gridding and interpolation technique selects the lowest LIDAR return within a specified search radius. As the search radius and cell size is increased, the probability of capturing a true ground also increases as more candidate LIDAR returns are considered. The minimum-bin technique is attractive because it is easy to implement and validate in the field. More complex methods (e.g. Sadro

et al., 2007), require resources and expertise beyond the scope of most regional or site-specific management (including restoration) efforts.

The objective of this research was to explore the accuracy of LIDAR-derived DEM as cell size is increased from 0.1 m to 6.0 m with a 0.1 m step size using the minimum-bin technique. LIDAR data was filtered with the minimum-bin technique to generate digital elevation models over a 174 ha tidal restoration site in the Pacific Northwest (PNW). The reference baseline was established using a high-resolution survey-grade RTK GPS survey (> 13000 measurements). By using this high-resolution RTK GPS survey, maps depicting the accuracy of LIDAR-derived DEM were generated to help reveal where the minimum-bin gridding method performed well and where further refinement or other interpolation methods may be more appropriate. This research contributes to a broader understanding of LIDAR error within tidal wetlands and to the Pacific Northwest where significant wetland restoration projects are taking place and are planned in the future.

2.3 Methods

2.3.1 Study Area

The study area for this research was the 174 ha Ni-les'tun Unit of the Bandon Marsh National Wildlife Refuge in the Coquille River Estuary, Oregon (Figure 2.1). The Coquille River Estuary is a drowned river mouth estuary with an area of 9.2 km^2 draining an area of 2731.5 km^2 with an average monthly river discharge of 70 $m^3 \cdot s^{-1}$ (Engle *et al.*, 2007; Bottom *et al.*, 1979). Elevations across the study area ranged from 0.6 m North American Vertical Datum of 1988 (NAVD88) to 13.4 m NAVD88, including a slope from the marsh plain to a road that borders the northern part of the marsh. The marsh plain made up the majority of the study area and had elevations between 0.9 m NAVD88 and 3.7 m NAVD88 with a mean of 1.95 m NAVD88. At the Ni-les'tun Unit study site, the Mean Higher High Water (MHHW) tidal datum was at an elevation of 2.17 m NAVD88 (Ewald, 2013a).

Ni-les'tun is a tidal wetland restoration site and is the largest tidal wetland restoration project implemented to date on the Oregon Coast. Construction began in 2009 and continued through late summer 2011. The site was originally converted from tidal wetland to agricultural pasture in the late 19th and early 20th century through diking and ditching to exclude tidal exchange within the boundaries of the site (Brophy and van de Wetering, 2012; Hawes *et al.*, 2008). Restoration actions undertaken to restore tidal flow included the removal or lowering of dike material along a natural levee, the removal of livestock, filling of more than 21 km of ditches, and the excavation of approximately 8 km of channels to facilitate tidal exchange within the site (Brophy and van de Wetering, 2012).

LIDAR and GPS survey of this site were conducted prior to restoration in 2009. At that time, muted tidal exchange was present due to the presence of fish-friendly tide gates (Brophy and van de Wetering, 2012). On the lower portions of the study area, the muted tidal exchange allowed development of native tidal marsh vegetation dominated by *Distichlis spicata* and *Carex lyngbyei* (Brophy and van de Wetering, 2012). On higher ground, vegetation communities were dominated by a mix of non-native pasture species (primarily *Festuca arundinacea* and *Agrostis stolonifera*, and *Lotus corniculatus*) and native tidal marsh species (primarily *Potentilla anserina* and *Juncus balticus*) (Brophy and van de Wetering, 2012). For more information about the condition of the study area at the time of survey, please refer to Brophy and van de Wetering (2012).

2.3.2 RTK GPS Survey

Ducks Unlimited surveyed the Ni-les'tun Unit study site in preparation for restoration design and implementation (Ducks Unlimited, 2010). LIDAR data was not available at the beginning of the design phase of the restoration project. As a result, Ducks Unlimited conducted a dense Real Time Kinematic (RTK) GPS survey of the site to provide an accurate elevation dataset for design and engineering. They followed GPS survey techniques that collected dense measurements in areas of

complex topography or engineering importance, while relying on sparser measurements in flat and even terrain. Both pole-mounted mobile (e.g., all terrain vehicle) and handheld RTK GPS measurements were collected using dual frequency GPS receivers capable of resolving centimeter-level horizontal and vertical accuracy in real time (Schulte, 2013).

The resulting dataset consisted of more than 18600 measurements. Of these, 13128 measurements that represented topographic features within the study area were selected from the dataset and used in the analysis presented in this paper. The data were collected in the NAD83(CORS96, Epoch 2002) Oregon State Plane South horizontal coordinate system, NAVD88 (GEOID03) vertical datum (Schulte, 2013). For the analysis presented in this paper, the GPS survey data were reprojected to Oregon State Plane Lambert (EPSG: 2992) to match the LIDAR dataset and the Oregon State coordinate system standard using ArcGIS (version 10.1) from Esri.

2.3.3 LIDAR Data

The Oregon LIDAR Consortium (OLC), led by the Oregon Department of Geology and Mineral Industries (DOGAMI), is a partnership between multiple state and federal agencies charged with coordinating, collecting, and disseminating LIDAR data throughout Oregon using consistent methods and quality assurance procedures. LIDAR point cloud and derived highest-hit and bare-earth raster models are now available for much of Western Oregon. To date, the OLC has acquired more than 69000 km^2 of LIDAR data with a minimum acceptable point density of 8.0 returns$\cdot m^{-2}$ over terrestrial surfaces (DOGAMI, 2013, 2008).

OLC partnered with The National Science Foundation (NSF) OpenTopography Facility (http://opentopography.org, NSF Award Numbers 0930731 and 0930643) to disseminate LIDAR point-cloud data. NSF OpenTopography archives all OLC LIDAR point-cloud data, and many other LIDAR datasets across the United States, and makes them available for download using convenient online query tools. NSF OpenTopography delivers the OLC LIDAR data in NAD83(CORS96, epoch 2002)

Oregon State Plane Lambert horizontal coordinate system and NAVD88 (GEOID03) vertical datum (Kleber, 2013).

2.3.3.1 Collection

LIDAR data used in this study was collected by a contractor (Watershed Sciences, Inc.) for OLC over the study area on June 14, 2008 as part of a large project (651 km^2) to map the South Coast of Oregon (Watershed Sciences, Inc., 2009a). The instrument used to perform the survey was a Leica ALS50 Phase II set to acquire data at ≥ 105000 pules per second at an altitude of 900 meters above ground level (AGL) with a scan angle of ±14°(field of view 28°) (Watershed Sciences, Inc., 2009a). These flight parameters yielded a swath width of 221 meters at ground level and a nominal spot diameter of 19.8 cm at nadir on flat topography (Watershed Sciences, Inc., 2009a). Flight path was structured to provide ≥ 50% side-lap between opposing flight-lines, yielding ≥ 100% total overlap to minimize the influence of laser shadowing and other artifacts (Watershed Sciences, Inc., 2009a). Aircraft altitude and position were measured by differential GPS on-board the aircraft twice per second and corrected using a network of survey-grade GPS receivers located at known benchmarks on the ground (Watershed Sciences, Inc., 2009a). The attitude of the aircraft was measured by an inertial management unit at 200 times per second (Watershed Sciences, Inc., 2009a). The LIDAR data was georeferenced and processed to align flight-lines, remove artifacts (e.g., birds), and classify ground points using TerraScan, TerraMatch, and proprietary tools developed by Watershed Sciences prior to delivery to DOGAMI (Watershed Sciences, Inc., 2009a). For more information about LIDAR data collection, please refer to Watershed Sciences, Inc. (2009a).

Within the Ni-les'tun Unit study area there were 12686962 LIDAR returns. Nearly all returns are first-return, with only 8172 second-returns, and 251 third-returns. 2841579 returns were classified as ground-returns, while the remaining 9845383 returns were left unclassified. The classification of LIDAR returns within

the dataset is of limited use for this study because the minimum-bin method relies only on selecting the lowest LIDAR return within a given area and does not use more complex filters or interpolators to derive a modeled ground surface.

2.3.3.2 Density

LIDAR returns across the Ni-les'tun Unit study area had a mean point density of 7.2 returns·m^{-2} (range: 0.0 returns·m^{-2} to 31.0 returns·m^{-2}), including terrestrial surfaces and open water regions near the tide gate. The highest point densities were in the overlap between 15 flight-lines which cover the site, while the lowest were over regions of the study area inundated with water at the time of acquisition (Figure 2.2).

2.3.3.3 Absolute Accuracy

Absolute vertical accuracy of LIDAR compares the elevation of a known elevation (e.g., survey-grade GPS measurement) to the nearest LIDAR laser point in open terrain with no obstructions to the ground surface. Watershed Sciences, Inc. (2009a) reports a fundamental vertical accuracy Root Mean Square Error (RMSE) of 4.5 cm (mean -1.5 cm, 4.6 cm standard deviation) on 12377 RTK GPS points collected on road surfaces spread across the extent of LIDAR collection. An independent dataset (109 measurements) collected by DOGAMI to perform quality assurance checks on the data found an RMSE of 5.8 cm (mean ± 4.7 cm, 3.4 cm standard deviation) (DOGAMI, 2009). To further validate the absolute accuracy, a subset of the RTK GPS survey that forms the base of the research presented in this paper was analyzed to compute the fundamental vertical accuracy of the LIDAR data. The estimated non-slope corrected absolute vertical RMSE of the LIDAR data is 10.4 cm (non-parametric bootstrapped 95% CI: 9.5 cm to 11.4 cm; R=10000 replicates) based on 294 independent RTK GPS measurements along a road bordering the study area which included two slopes of up to ± 10 degrees. Similarly, the estimated non-slope corrected vertical Mean Absolute Error (MAE) of the LIDAR data is 8.1 cm (non-parametric bootstrapped 95% CI: 7.4 cm to 8.9 cm; R=10000 replicates) over

the same dataset. Differences between these estimates of absolute LIDAR accuracy can be explained by examining a small subset of the overall LIDAR collection area for this study, the use of differing topography, survey equipment, survey date and times that result in different satellite geometries for each survey.

2.3.4 DEM Generation & Performance

Digital elevation models (DEMs) were generated from the LIDAR using the Geoscience Network (GEON) Points2Grid Utility (version 1.0.1, available at http://opentopography.org/index.php/Tools/otforge/points2grid) with cell sizes ranging from 0.1 m to 6.0 m (0.01 m^2 to 36.00 m^2) and a step size of 0.1 m, yielding 60 DEM candidates to evaluate model performance. When generating these DEMs, both unclassified and ground-classified LIDAR returns were considered, and each DEM shared the same spatial extent and was created using the same source LIDAR data.

To evaluate the accuracy of each candidate DEM, the raster DEM was queried at the spatial location of each RTK GPS point. The difference between the LIDAR-derived DEM elevation (H_{LIDAR}) and the RTK GPS surveyed marsh surface elevation (H_{GPS}) is the LIDAR-GPS discrepancy (see Eq. 2.1).

$$D = H_{LIDAR} - H_{GPS} \tag{2.1}$$

LIDAR-GPS discrepancy (D) is consistently reported in centimeters and calculated from spatial data referenced in the same horizontal datum, vertical datum, and the NOAA National Geodetic Survey (NGS) GEOID03 geoid model.

Two common magnitude-based measures of model performance are Root Mean Squared Error (RMSE) and Mean Absolute Error (MAE) (Willmott and Matsuura, 2005). RMSE and MAE are defined in Equations 2.2 and 2.3 below, where H_{LIDAR} and H_{GPS} are the orthometric heights of a location derived from LIDAR and RTK GPS, respectively.

$$RMSE = \sqrt{\frac{1}{n}\sum_{i=1}^{n}(H_{LIDAR} - H_{GPS})^2} \quad (2.2)$$

$$MAE = \frac{1}{n}\sum_{i=1}^{n}|H_{LIDAR} - H_{GPS}| \quad (2.3)$$

RMSE, MAE, mean discrepancy, and standard deviation were calculated for each cell size candidate DEM using the full dataset of 13128 RTK GPS measurements as the *true* (i.e., observed) ground surface. The RTK GPS measurements were assumed to have zero horizontal or vertical error. The LIDAR-derived DEM elevation was the *predicted* elevation. In reality, the GPS data are not error-free, but are more accurate than the LIDAR data in both horizontal and vertical coordinates. The data was bootstrapped using a basic nonparametric method and 100000 replicates to derive confidence intervals for each metric (Canty and Ripley, 2013; Davison and Hinkley, 1997).

RMSE is often misinterpreted because it is sensitive to the variability within the magnitude and distribution of discrepancies between predicted and observed values (Willmott and Matsuura, 2005). Therefore, MAE is the preferred model performance metric for the purposes of selecting the best performing cell size. RMSE and MAE are reported throughout the body of this research to aid in the comparison with other studies.

The *gstat* package in the R statistical environment was used to interpolate LIDAR-GPS discrepancy across the study area for select cell sizes using an inverse distance weighted (IDW) interpolation technique and a 5.0 m cell size (R Core Team, 2012; Pebesma, 2004). These visualizations aid in the interpretation of RMSE, MAE, and the other performance metrics.

2.4 Results

DEM accuracy increased with cell size until an inflection point near 1.4 m as the influence of vegetation is mitigated by the minimum-bin gridding technique (Figure 2.3a). Low features within the landscape were captured by the gridding technique and degrade DEM performance after cell size enlarged beyond the optimum. Minimizing MAE yielded ([1] in Table 2.1) an optimum cell size of 1.4 m (1.92 m^2) for this dataset. If RMSE ([2] in Table 2.1) was used to define the optimum DEM cell size instead of MAE, the optimum cell size was 1.2 m (1.44 m^2). LIDAR-GPS discrepancy derived from a DEM with a cell size of 1.4 m falls 2.9 cm below, and is statistically different from, a cell size of 1.2 m (two-sided paired t-test: p-value < 0.001, 95% CI: -3.1 cm to -2.7 cm). Mean LIDAR-GPS discrepancy is positive for both cell sizes. A cell size of 1.4 m yields a statistically significant mean positive bias of 1.6 cm above known elevation (two-sided t-test: p-value < 0.001, 95% CI: 0.9 cm to 2.3 cm). A cell size of 1.2 m yields a statistically significant mean positive bias of 4.5 cm above known elevation (two-sided t-test: p-value < 0.001, 95% CI: 3.8 cm to 5.2 cm).

Even at the optimum cell size, the DEM is still positively biased when compared to known ground elevations. Mean LIDAR-GPS discrepancy remains positive until a cell size of 1.6 m is achieved. At cell sizes greater than 1.6 m, DEM are negatively biased as the minimum-bin method continues to capture and favor low features within the landscape. Median and mean LIDAR-GPS discrepancy fall with increasing cell size (Figure 2.3b).

Figure 2.4 reveals the spatial pattern of LIDAR-GPS discrepancy across the study area. Minimum-bin LIDAR-derived DEM elevations underpredict (typically 70 cm to 90 cm below) the measured elevation along channels and the man-made dike that form the southern edge of the site adjacent to the Coquille River. These features are characterized by high ground, a moderate to steep slope, and low ground over a short horizontal distance. For example, the minimum-bin filter is likely to

select a LIDAR return from an adjacent low riverbank rather than the surveyed wetland surface. The likelihood of upslope areas being assigned an elevation lower than the true ground elevation increases as the cell size is increased.

The minimum-bin LIDAR-derived DEM overpredicted elevations in the northwestern (NW) quadrant of the study area (Figure 2.4). Overprediction is most pronounced at small cell sizes and decreases with increasing cell size. Even at the maximum cell size of 6.0 m, regions within the NW quadrant are still positively biased (typically 50 cm to 70 cm) where vegetation is characterized by dominant *Carex obnupta* with 100% cover (Brophy and van de Wetering, 2012).

Figure 2.5 plots regions within the study area that have a mean LIDAR-GPS discrepancy within ± the upper 95% confidence limit (8.9 cm) of absolute MAE of the LIDAR system as evaluated using RTK GPS points with open sky conditions along the road bordering the study area. The highest percentage of the study area (58%) is within the MAE 95% confidence interval with a cell size of 2.0 m. At cell sizes smaller than 2.0 m, the percentage of the site that falls within the 95% confidence interval range quickly increases. At cell sizes greater than 2.0 meters, the proportion of the site that falls within the upper limit of the MAE 95% confidence interval slowly falls (Figure 2.3d).

At small DEM cell sizes, most of the study area is outside the 95% MAE absolute vertical accuracy threshold (Figure 2.3d). As cell size is increased, areas near channels and low vegetation transition to within 95% MAE absolute vertical accuracy threshold. At cell sizes near 2.0 m, regions of the DEM that lie near channels and ditches fall outside the acceptable MAE range, because low features in the landscape are favored by the minimum-bin method. This trend continues throughout the larger cell sizes and is most pronounced at the 6.0 m cell size (Figure 2.5).

2.5 Discussion

DEM accuracy initially increases as cell size is increased from 0.1 m to an optimum of 1.4 m as the effect of dense vegetation is mitigated by the minimum-bin

gridding method. After the optimum cell size is reached and cell size is increased further, DEM accuracy begins to degrade as the gridding method captures and favors low features (e.g., channels) in the landscape. This pattern occurs because more LIDAR return samples are available to the minimum-bin filter as cell size increases, thereby increasing the probability of one of those returns capturing the true ground elevation within the search radius instead of hitting vegetation. However if the cell size is too large, the DEM will be biased towards low features because many of the LIDAR samples around each DEM raster pixel centers include a return that represents the elevation of a channel or other low feature at the edge of the search radius.

Figure 2.6 presents the density distribution of LIDAR-GPS discrepancy measurements for DEM with cell sizes of 0.5 m, 1.4 m (optimum DEM), 4.0 m, and 6.0 m. The ideal distribution is centered on zero with a symmetric rise and fall. A DEM generated with a cell size of 0.5 m has the highest density of LIDAR-GPS discrepancy around 15 cm and is skewed toward the right. The MAE-minimized optimum DEM with a cell size of 1.4 m has the narrowest spread of any considered cell size and is symmetric around the median LIDAR-GPS discrepancy, 6.4 cm. At larger cell sizes, the distribution widens further and the peak shifts to the left. Wider and flatter distributions indicate that the DEM is less accurate for a given measurement location. This trend can also be observed in the standard deviation of LIDAR-GPS discrepancy (Figure 2.3c). Standard deviation is high throughout the range of considered cell sizes. As cell size is increased, changes to standard deviation of LIDAR-GPS discrepancy are a function of both a wide range of discrepancies and variable performance of the minimum-bin technique. All 13128 RTK GPS measurements in the dataset are considered to evaluate vertical accuracy for each candidate DEM. Therefore, a small subset of LIDAR-GPS discrepancy measurements may stand in stark contrast to the majority of other discrepancies and these measurements will act as influential data points to increase the standard deviation. A minimum standard deviation LIDAR-GPS discrepancy value of 38.8 cm occurs at a cell size of 1.2 m, consistent with the optimum DEM cell size as obtained by

minimizing RMSE. Standard deviation of LIDAR-GPS discrepancy falls rapidly at cell sizes smaller than this value and rises quickly at cell sizes greater than 1.2 m.

A high-quality DEM for quantitative analysis approximates the true elevation at a given location and the topography around it. Ideally, the DEM will reveal breaks in the topography such as small channels and ridges. A disadvantage of the minimum-bin filter is that at large cell sizes, small breaks in topography are lost within the landscape (Schmid *et al.*, 2011). For example, at a cell size of 6.0 m any low LIDAR return within 6.0 m of a given location will be selected for that pixel elevation. This has the effect of increasing the modeled size of a 0.5 m wide channel that represents the low feature within the search radius. Any pixel center that is within a radius of 6.0 meters would inherit a low-elevation LIDAR return that fell within the channel. The mean DEM-derived elevation within the 6.0 m search radius would be negatively biased towards the low channel elevations. More advanced LIDAR return classifiers, especially classifiers that examine the slope and shape of topography around a given area, are more likely to accurately model the topography as well as elevation across the landscape (Briese, 2010). Therefore, minimizing the cell size when employing the minimum-bin technique is desirable to retain small topographic features in the landscape and prevent exaggeration of low features.

The success of a LIDAR system for creating a DEM is dependent on capturing LIDAR returns that represent the ground surface while removing bias from vegetation. If LIDAR laser pulses are unable to reach the ground there is little chance of success for a LIDAR classification and interpolation strategy. Even the minimum-bin method, which selects the lowest return within the search radius, will overestimate the ground surface. High return density LIDAR is more likely to provide a LIDAR return representing the ground because there are more returns per unit area. The Ni-les'tun Unit LIDAR survey has a mean point density of 7.2 returns$\cdot$m^{-2} (range: 0.0 returns$\cdot$m^{-2} to 31.0 returns$\cdot$m^{-2}) when compared against other studies, which typically range between 0.7 returns$\cdot$m^{-2} and 4.0 returns$\cdot$m^{-2} (Schmid *et al.*, 2011; Chassereau *et al.*, 2011; Hladik and Alber, 2012; Wang *et al.*, 2009).

Despite the use of higher LIDAR return density data, the Ni-les'tun LIDAR survey shows evidence of a positive bias in the region dominated by *Carex obnupta* (NW corner of Figure 2.4).

The data presented in this paper is consistent with past research. A cell size of 1.4 m (1.96 m^2) provided the best accuracy, yielding an MAE of 24.3 cm (RMSE 39.7 cm) and a mean positive bias of 1.6 cm. Schmid *et al*. (2011) considered cell sizes of between 2.0 m and 10.0 m, selecting an optimal cell size of 4.0 m in *Spartina alterniflora* and a cell size of 10.0 m in *Juncus roemerianus* by minimizing the Root Mean Square Error (RMSE) on 280 survey-grade GPS measurements in South Carolina. Wang *et al*. (2009) used 240 survey-grade GPS measurements and cell sizes between 0.5 m and 6.5 m, finding that an optimum cell size of 3.5 m by minimizing the overall RMSE on a dataset with vegetation dominated by *Spartina maritima*, *Sarcocornia fruticosa*, *Limonium narbonense*, and *Juncus maritimus*. The minimum-bin method was successful in mitigating much of the vegetation bias within DEM and the optimum cell size for the Ni-les'tun LIDAR dataset is much smaller than past studies have found. This may be the result of higher LIDAR-density, dense ditch networks, or different vegetation communities from past studies.

2.6 Conclusion

The results of this investigation yield new information about the effect of cell size on LIDAR-derived DEM accuracy. The minimum-bin method successfully mitigated positive bias in DEM caused by dense vegetation. Optimum cell size for the Ni-les'tun Unit dataset is 1.4 m (1.96 m^2). Mean absolute error at this cell size was 24.3 cm with a mean bias of 1.6 cm. At cell sizes smaller than the optimum, LIDAR-derived DEM are positively biased due to dense vegetation interference. At cell sizes larger than the optimum, channels and other low features within the search radius are assigned to raster DEM cell center thereby negatively biasing the DEM. Understanding vertical elevation uncertainty in LIDAR data is a critical challenge facing environmental analysis and management strategies. Small errors in an

elevation model could lead to significant differences in the products of analysis, which in turn may lead to the development and implementation of policy and management strategies based on faulty or inaccurate data. Further research is needed to understand how existing LIDAR filtering and interpolation strategies behave in a variety of landscapes and vegetation communities.

2.7 Acknowledgments

This research would not have been possible without the contributions of a variety of partners. Thank you to Ducks Unlimited, U.S. Fish and Wildlife Service, The Estuary Technical Group of the Institute for Applied Ecology, and Green Point Consulting for providing data. GeomaticsResearch provided technical and computing resources. The Marine Resource Management Program at Oregon State University's College of Earth, Ocean, and Atmospheric Sciences provided financial and a variety of other assistance. Guidance and mentorship from Laura Brophy, Jim Graham, and Michael Olsen was instrumental in the success of this research.

2.8 Tables and Figures

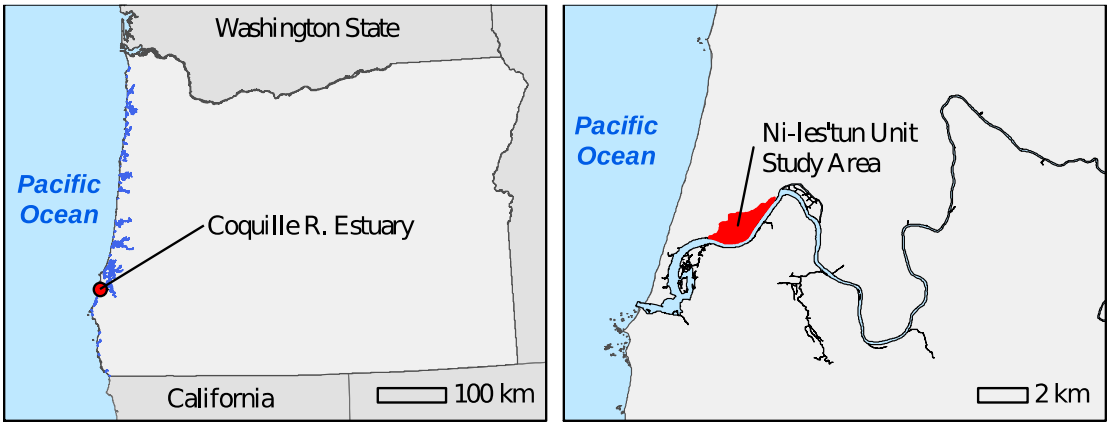

Figure 2.1: Minimum-bin study area map. The study area for this research is the Ni-les'tun Unit of the Bandon Marsh National Wildlife Refuge in the Coquille River Estuary, Oregon, USA.

Figure 2.2: LIDAR density across the Ni-les'tun Unit study area. The mean LIDAR return density is 7.2 returns·m^{-2}. The horizontal coordinate system is Oregon Statewide Lambert (EPSG: 2992; units: International Feet).

Table 2.1: DEM model performance metrics. Cell size is reported in meters, all other units are in centimeters. [1] optimum RMSE cell size. [2] optimum MAE cell size.

Cell Size	MAE	RMSE	% Valid	Mean_± SE	SD	Median	1st Qu.	3rd Qu.
0.2	39.73	63.98	6.68	32.38 ± 0.51	55.18	22.10	10.36	45.72
0.5	30.65	47.89	21.54	19.24 ± 0.38	43.85	14.94	5.18	32.61
1.0	25.46	39.94	39.63	7.84 ± 0.34	39.17	9.75	-0.30	22.66
1.2 [1]	24.48	39.09	45.71	4.50 ± 0.34	38.84	7.93	-2.44	19.51
1.4 [2]	24.27	39.65	50.80	1.62 ± 0.35	39.61	6.40	-4.57	17.37
1.5	24.30	40.09	52.89	0.29 ± 0.35	40.09	5.79	-5.95	16.46
2.0	25.54	43.52	57.68	-5.62 ± 0.38	43.15	3.05	-12.31	13.11
4.0	33.79	59.91	53.28	-20.25 ± 0.46	53.19	-4.88	-31.09	7.62
6.0	40.29	65.19	44.88	-29.56 ± 0.51	58.10	-12.19	-44.20	3.87

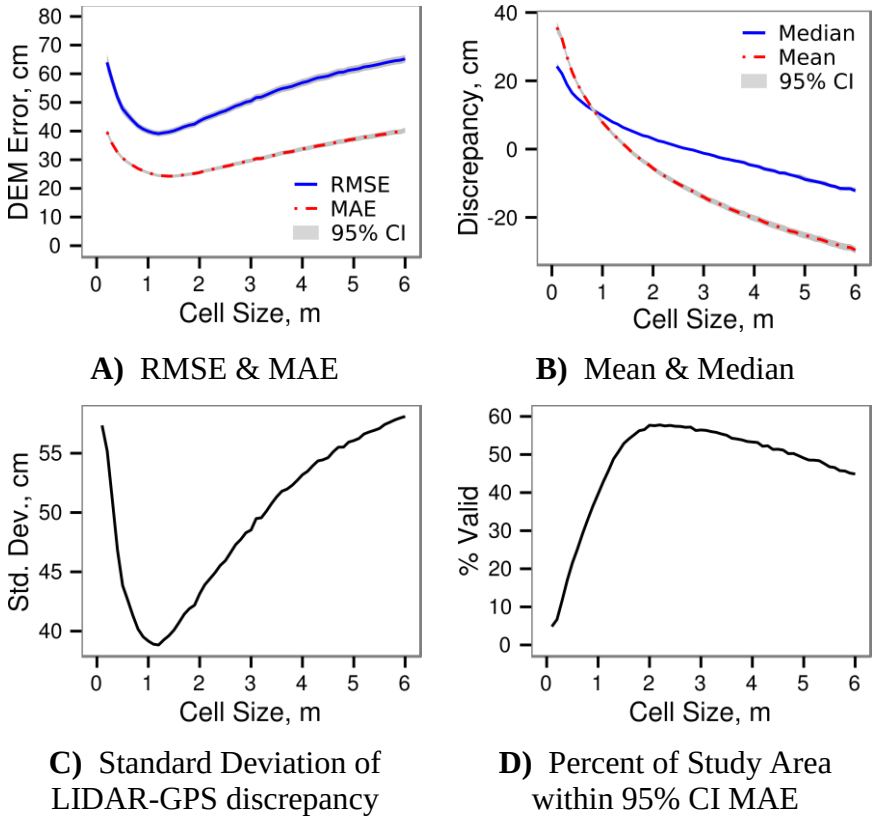

A) RMSE & MAE

B) Mean & Median

C) Standard Deviation of LIDAR-GPS discrepancy

D) Percent of Study Area within 95% CI MAE

Figure 2.3: Minimum-bin DEM calibration plots. DEM performance diagnostic metrics with cell sizes of 0.1 m to 6.0 m, with a 0.1 m step size. Confidence intervals were generated from a non-parametric bootstrap with 5000 iterations.

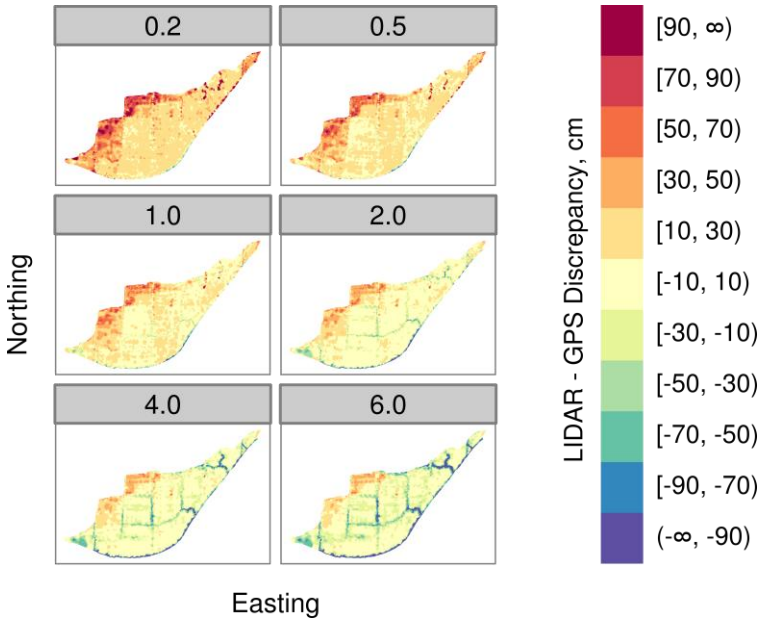

Figure 2.4: LIDAR-GPS discrepancy spatial distribution. This figure plots the difference between LIDAR-derived DEM elevations and measured RTK GPS elevations across the site and interpolated using IDW. Each facet of the figure represents a different cell size, ranging from 0.2 m to 6.0 m.

Figure 2.5: DEM accuracy thresholds. Each facet of the figure represents the cell size in meters.

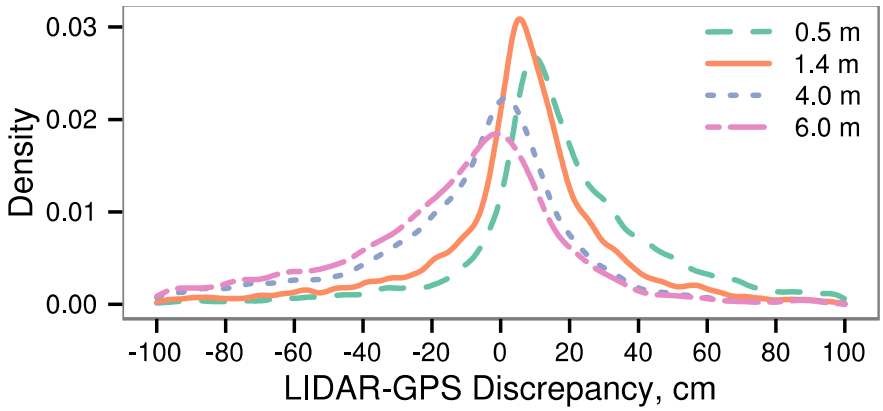

Figure 2.6: Density distribution of LIDAR-GPS discrepancy for selected cell sizes. The distribution of discrepancies is unimodal throughout their range. The figure extents are truncated to within 100 cm of zero. Density represents the probability of a given discrepancy based on all 13128 LIDAR-GPS discrepancy measurements.

CHAPTER 3

LIDAR INTERFERENCE BY VEGETATION IN OREGON TIDAL MARSH DIGITAL ELEVATION MODELS

Michael J. Ewald

Marine Resource Management Program
Oregon State University
Corvallis, Oregon

Laura S. Brophy

Estuary Technical Group
Institute of Applied Ecology
Corvallis, Oregon

Christopher N. Janousek

Western Ecology Division
US Environmental Protection Agency
Corvallis, Oregon

November 18, 2013

CONTRIBUTION OF AUTHORS

Michael J. Ewald, the primary author of this publication, developed the methodology, performed all analysis, interpreted results, and wrote the text.

Laura S. Brophy helped develop the research objectives, provided data, assisted with interpretation of the results, and contributed revisions to this document. Laura provided guidance and mentorship throughout the duration of my thesis as my primary advisor.

Christopher N. Janousek provided data and guidance on methods development and interpretation. Christopher's datasets doubled the data available for this project and he provided critical statistical guidance and interpretation.

3 LIDAR INTERFERENCE BY VEGETATION IN OREGON TIDAL MARSH DIGITAL ELEVATION MODELS

3.1 Abstract

Light Detection and Ranging (LIDAR) is a powerful resource for coastal and wetland managers and its use is increasing. Vegetation density and other land cover characteristics influence the accuracy of LIDAR-derived ground surface digital elevation models; however the degree to which wetland land cover biases LIDAR estimates of the ground surface is largely unknown. We investigated LIDAR interference by tidal vegetation across six Oregon estuaries and twelve common wetland types using survey-grade Global Positioning System (GPS) measurements of the wetland surface and quantitative vegetation data (percent cover by species) for each measurement location. Our results show that LIDAR estimates of the ground surface are typically 10 cm to 30 cm above GPS measurements of the wetland surface in Oregon tidal wetland plant associations. Plant associations dominated by *Carex obnupta* and *Carex lyngbyei* exhibited the largest discrepancy between GPS and LIDAR measurements (mean discrepancies 36.6 cm and 48.8 cm respectively). The smallest errors observed in the study were about 10 cm and occurred in two low tidal marsh associations dominated by *Deschampsia cespitosa*, *Distichlis spicata*, *Sarcocornia perennis* and *Jaumea carnosa*. Our research yields new information for coastal LIDAR users, increases our understanding of uncertainty in LIDAR-derived datasets, and improves our ability to accurately evaluate and manage coastal environments.

3.2 Introduction

Coastal zones are challenging to manage because of their complexity (Shackeroff *et al.,* 2009; Guichard and Peterson, 2009). Holistic coastal management policies have gained popularity, but require the adoption of complex spatial

modeling, planning, and mapping technologies and techniques (Ricketts, 1992; Brock and Purkis, 2009). New models seek to identify the extent of tidal influence, predict the effect of different sea-level rise scenarios, map habitats, and many other tasks that have direct implications on coastal communities and ecosystems (Brock and Purkis, 2009). The shift to managing the environment as a system instead of discrete elements is exciting, and reflects the principles of Ecosystem Based Management (McLeod and Leslie, 2009).

Increased reliance on complex models and analysis requires accurate and complete source data (Palmer, 2009; Simenstad *et al.*, 2005). While geospatial technologies and techniques such as LIDAR (Light Detection And Ranging) are potentially more accurate than some other methods, they are far from perfect. Unfortunately, GIS (Geographic Information Sciences) does a poor job of identifying, communicating, and propagating uncertainty (Couclelis, 2003). Uncertainty is a challenge to EBM approaches that rely on comprehensive modeling and management strategies rooted in data. Understanding and communicating uncertainty within digital elevation models (DEM) is critical to the success of inquiry and analysis of coastal ecosystems for both science and management purposes. For example, LIDAR data is heavily used within tidal wetland restoration and management at both local and regional spatial scales. In coastal zones, environmental conditions and floristic development are often strongly associated with elevation (Odum, 1985, 1988; Cornu and Sadro, 2002; Brock and Purkis, 2009). Strong associations require high resolution and accurate elevation data to accurately model and predict outcomes of management intervention (Simenstad *et al.*, 2005; Cornu and Sadro, 2002; Kentula, 2000). Plant communities are very sensitive to small changes in elevation; a difference of a few centimeters in elevation between sites causes differences in tidal hydrology and therefore plant community composition (Odum, 1985, 1988; Cornu and Sadro, 2002).

Airborne LIDAR is a remote sensing technology that uses a laser scanner mounted on an aircraft to scan the surface of the earth. Many LIDAR data collection parameters determine the LIDAR pulse return density and success of the system in

mapping terrains including aircraft altitude, LIDAR sensor, flight altitude, swath width, pulse width, pulse frequency, and many others (Hodgson and Bresnahan, 2004; Wehr and Lohr, 1999). Additionally, filtering and interpolation techniques used to transform as-received LIDAR point-cloud data to a raster-based DEM influence the accuracy and efficacy of models for a particular purpose (Meng *et al.*, 2010; Bater and Coops, 2009; Wehr and Lohr, 1999). The absolute vertical accuracy, the ability to accurately measure elevation in ideal conditions, is on the order of 5 cm to 20 cm for modern instruments (Beraldin *et al.*, 2010). The error budget within a LIDAR dataset is more difficult to quantify and dependent on land cover class (Beraldin *et al.*, 2010; Briese, 2010). For example, LIDAR filters and classifiers are well suited for removing buildings and trees from a DEM where separation between ground and other landscape features is significant (Briese, 2010; Meng *et al.*, 2010). The filters are not as effective in large regions covered by a consistent patch of dense grass or other land-cover where separation between ground points and features on the surface is minimal (Briese, 2010; Meng *et al.*, 2010). Yet, the influence of specific tidal wetland vegetation on the quality of LIDAR-derived DEM is currently unknown.

Past research has shown that estimated ground surface elevation from raster-based LIDAR-derived DEM are typically higher than surveyed elevations using survey-grade Global Positioning System (GPS) measurements of the tidal wetland ground surface (Schmid *et al.*, 2011; Chassereau *et al.*, 2011; Hladik and Alber, 2012; Athearn *et al.*, 2010; Wang *et al.*, 2009; Sadro *et al.*, 2007; Montané and Torres, 2006; Rosso *et al.*, 2006). Most studies of LIDAR error have focused on *Spartina spp.* dominated tidal wetlands along the Atlantic and Gulf coasts of the United States. Additional research has been undertaken in San Francisco Bay (Athearn *et al.*, 2010), Italy (Wang *et al.*, 2009), and Denmark (Moeslund *et al.*, 2011). In these studies, the mean difference between LIDAR-derived elevations and GPS-surveyed elevations is between 10 cm and 45 cm. Micro-topography within the LIDAR spot diameter does not significantly affect LIDAR error (Montané and

Torres, 2006). Hladik and Alber (2012) found that vegetation height was correlated with LIDAR error but that the difference between LIDAR-derived elevations and true elevation was less than the total vegetation canopy height. Wang *et al.* (2009) found the bias was correlated with basal leaves and other low elements in herbaceous wetlands.

Considerable research has attempted to quantify LIDAR error in tidal wetlands, and subsequently to apply DEM correction factors to mitigate the influence of vegetation (Montané and Torres, 2006; Wang *et al.*, 2009; Hladik and Alber, 2012). Hladik and Alber (2012) successfully developed correction factors for the main vegetation types within their study area using a field survey to map vegetation communities. Sadro *et al*. (2007) employed hyper-spectral remote sensing to map vegetation communities and developed species-specific correction factors. Schmid *et al*. (2011) and Wang *et al*. (2009) employ a minimum-bin gridding technique to identify the optimum search radius for ground LIDAR returns and interpolate a raster DEM from the LIDAR point cloud. While these studies, and our own, yield important information about the performance of LIDAR within tidal wetlands, they are specific to the wetlands and vegetation communities they sampled. Oregon wetlands differ significantly from the ecosystems studied previously; hence past research may not be applicable to this region. In Oregon, tidal wetlands are often heavily influenced by wintertime fluvial input driven by heavy rain (Lee *et al.*, 2009; Engle *et al.*, 2007; Bottom *et al.*, 1979). Low marsh is typically dominated by *Jaumea carnosa*, *Distichlis spicata*, and *Salicornia perennis* (Jefferson 1975; Brophy *et al.*, 2011). High marsh is more abundant in Oregon and is characterized by *Deschampsia cespitosa*, *Potentilla anserina*, *Agrostis stolonifera*, and *Juncus balticus* (Jefferson, 1975; Seliskar and Gallagher, 1983; Brophy *et al.*, 2011).

The objective of this research is to explore the LIDAR-derived DEM error of 12 typical Oregon tidal wetland vegetation communities. High-accuracy GPS survey techniques and co-located vegetation surveys identify the marsh plain elevation and species-level quantitative vegetation cover at each measurement location. The results

of this analysis complement existing research by adding data from the Pacific Northwest, United States across a variety of study areas and vegetation communities along the Oregon coast.

3.3 Methods

3.3.1 Study Areas

The study area for this research consists of high, mid, and low tidal marsh sites and one tidal wetland restoration site within six Oregon estuaries, compiled from the data of Janousek and Folger (2013), Brophy and van de Wetering (2012), and Brophy *et al*. (2011). These estuaries include Netarts Bay Estuary, Siletz River Estuary, Yaquina River Estuary, Alsea River Estuary, Coos Bay Estuary, and the Coquille River Estuary (Figure 3.1).

The geomorphic settings for five of the six estuaries in this study are drowned river mouth estuaries, a type that is common in Oregon (Lee *et al.*, 2009; Bottom *et al.*, 1979). Netarts Bay differs from the others and represents a bar built estuary (Lee *et al.*, 2009; Bottom *et al.*, 1979). Drowned river mouth estuaries refer to a river where current sea level has flooded the river mouth following sea level rise at the end of the last ice age (Bottom *et al.*, 1979). Heavy rainfall and small watershed size lead to significant wintertime freshwater input to the estuary (Lee *et al.*, 2009; Engle *et al.*, 2007; Bottom *et al.*, 1979). Tidal range is between 1.6 m and 1.9 m and varies by estuary (Lee *et al.*, 2009).

3.3.2 Field Survey

Janousek and Folger (2013), Brophy and van de Wetering (2012), and Brophy *et al*. (2011) conducted fieldwork as part of their studies and we compiled their data for the work presented in this paper (Table 3.1). Measurements included a quantitative survey of species-level percent cover within a one square meter quadrat and high-accuracy survey-grade elevation survey of the marsh plain elevation. Elevation information was used within these studies to relate tidal hydrology to other

physical site characteristics, and to relate physical drivers to floristic development and other biotic responses (Janousek and Folger, 2013; Brophy and van de Wetering, 2012; Brophy *et al.*, 2011). Janousek and Folger (2013) and Brophy *et al*. (2011) characterized least-disturbed tidal wetlands in multiple estuaries on the Oregon coast. Both Janousek and Folger (2013) and Brophy and van de Wetering (2012) collected data in the Coquille River Estuary. Brophy and van de Wetering (2012) collected measurements at 213 locations within a wetland restoration project at the Ni-les'tun Unit of the Bandon Marsh National Wildlife Refuge, the largest tidal wetland restoration project implemented to date on the Oregon Coast. Data were collected prior to restoration in this diked former tidal wetland; the pre-restoration vegetation communities consisted of non-native pasture species intermixed with native tidal marsh species. Brophy and van de Wetering (2012) also collected data at 60 locations in a least-disturbed mid to high elevation tidal marsh reference site, also located within the Bandon Marsh National Wildlife Refuge.

3.3.2.1 Vegetation Data

Trained botanists and ecologists familiar with Pacific Northwest tidal wetland species assemblages performed quantitative surveys of vegetation at each measurement location. These surveys used a one square meter quadrat placed along a transect or located using a stratified random sample design (Janousek and Folger, 2013; Brophy and van de Wetering, 2012; Brophy *et al.*, 2011). Janousek and Folger (2013) used stratified random sampling to select quadrat locations. Brophy and van de Wetering (2012) and Brophy *et al*. (2011) measured vegetation in randomly placed quadrats within transects placed in representative major vegetation communities and physical environmental settings.

At each vegetation survey location, the percent cover of each species within the quadrat frame was estimated and recorded. Janousek and Folger (2013) estimated the Relative Percent Cover, the per-species percent cover of only the uppermost layer of vegetation. Therefore, bare ground plus total plant cover always summed to 100%.

Brophy and van de Wetering (2012) and Brophy *et al*. (2011) also estimated the cover of each species within the quadrat but considered layering of multiple species (Absolute Percent Cover), allowing total plant cover to exceed 100%. Cover of bryophytes and macroalgae were measured by Janousek and Folger (2013) but not by Brophy et al. (2011) or Brophy and van de Wetering (2012). For our study, we included bryophyte and macroalgae cover estimates as part of bare ground cover for three reasons: they were unlikely to significantly bias LIDAR due to their low growth forms and short height, they were rare within the dataset, and their coverage was always low (< 10 percent cover).

While similar, the use of Absolute Percent Cover and Relative Percent Cover precludes direct comparison between vegetation data. To allow direct comparison, we adjusted the Absolute Percent Cover values for each species proportionately to create equivalent estimated Relative Percent Cover values for the vegetation data of Brophy and van de Wetering (2012) and Brophy *et al*. (2011). The result, Relative Percent Cover from Absolute Cover (C_{RFA}, Eq. 3.1), was approximately equivalent to the data of Janousek and Folger (2013).

$$C_{RFA} = C_A * \frac{TRPC_{est}}{TAPC} \tag{3.1}$$

$$TRPC_{est} = \begin{cases} 100, & TAPC \geq 100 \\ TAPC, & TAPC < 100 \end{cases} \tag{3.2}$$

$$TAPC = \sum C_A \tag{3.3}$$

For each vegetation plot, the absolute percent cover measurement for a given species (C_A) was multiplied by the ratio of estimated Total Relative Percent Cover ($TRPC_{est}$, Eq. 3.2) over Total Absolute Percent Cover (TAPC, Eq. 3.3). If TAPC was less than 100%, the sum of all species present in the plot (TAPC, Eq. 3.3) was assigned as the value of $TRPC_{est}$. If TAPC was greater than or equal to 100%, the entire plot is covered by vegetation, and 100% is assigned as the value of $TRPC_{est}$.

The aggregated vegetation dataset from Janousek and Folger (2013), Brophy and van de Wetering (2012), and Brophy *et al*. (2011) included 77 species. The most abundant species in the dataset were *Agrostis* spp., *Juncus balticus*, and *Potentilla anserina*. Thirty-eight species were rare within the dataset (fewer than 10 observations and cover never exceeded 20%). The top thirty-nine species and percent cover of bare ground were used for analysis.

3.3.2.2 Vegetation Plot Horizontal Coordinates

We assigned Cartesian coordinates to each of the vegetation plots using two methods, direct measurement and distance along a transect baseline. Janousek and Folger (2013) directly measured the Cartesian coordinates of each vegetation plot using Real Time Kinematic (RTK) GPS. Their data was reported in North American Datum of 1983 (NAD83) Universal Transverse Mercator Zone 10 North (UTM Zone 10N, EPSG: 26910). Brophy and van de Wetering (2012) and Brophy *et al*. (2011) located vegetation plots along transects. Each end of the transect was positioned in the NAD83 UTM 10N coordinate system coordinates using an RTK GPS receiver and monumented with a permanent marker (metal fencepost driven 60-100 cm into the soil). Individual vegetation plots were located in the UTM 10N coordinate system using a distance along the baseline between the transect ends, a known transect start end, and a constant one meter offset perpendicular to the baseline (Brophy and van de Wetering, 2012; Brophy *et al.*, 2011).

The horizontal coordinates of each vegetation plot were reprojected from UTM 10N to Oregon State Plane Lambert (EPSG: 2992) using ArcGIS 10.1 (version 10.1, http://esri.com) from Esri. This was necessary to match the LIDAR data and other datasets used in our analysis and interpretation.

3.3.2.3 Elevation Survey

All three studies that provided data for our analysis employed survey-grade GPS measurement techniques to generate accurate measurements of the ground

surface elevation near vegetation survey locations. Janousek and Folger (2013) measured the elevation of each vegetation plot using a Trimble 4700 GPS receiver and rapid static GPS survey methods. The vertical error of their measurements was between 0 cm and 4 cm (Std. Dev.: 1.2 cm), computed from the elevation difference between repeated GPS measurements of the National Geodetic Survey (NGS) benchmark at South Beach, Oregon (Janousek and Folger, 2013). RTK GPS surveying for Brophy and van de Wetering's (2012) vegetation transects was conducted using RTK GPS techniques on a pole-mounted roving receiver (Pat Schulte, Ducks Unlimited, personal communication). We recovered and resurveyed local benchmarks established during the original survey and found a vertical error of less than 5 cm. Brophy *et al*. (2011) collaborated with NOAA National Geodetic Survey (NGS) for their survey, established local geodetic control, and were successful in mapping the wetland surface in their study, however they did not report vertical accuracy for their RTK GPS survey. The NGS team collected rapid-static GPS occupations (processed using NOAA Online Positioning User Service) of benchmarks throughout the study area and found an overall error of less than 2 cm. In all studies used in our analysis, experienced GPS field crews performed the survey, established local geodetic control, and employed modern RTK GPS and rapid-static receivers capable of centimeter-level measurements (Janousek and Folger, 2013; Brophy and van de Wetering, 2012; Brophy *et al.*, 2011).

The elevation of most of our vegetation plots was not directly measured using a GPS at the center of the plot. Therefore, we created a Triangulated Irregular Network (TIN) DEM to compare GPS-surveyed elevation at each vegetation plot to LIDAR-derived DEM and point cloud measurements. TIN DEM linearly interpolate between RTK GPS measurements (i.e., vertices of the TIN) to build a DEM without constraining the data to a rectangular raster format. Vertical relief within Oregon tidal wetlands is minimal and all vegetation plots had multiple GPS measurements within 10 m. Interpolation effects to be minimal and our final TIN accuracy is sufficient for our purposes.

3.3.3 Vegetation Associations

We assigned vegetation association memberships to each vegetation plot by grouping the quantitative vegetation data into twelve distinct clusters. Clustering the data is needed to reduce the effects of colinear relationships between species that aggregate together on the landscape (McCune *et al.,* 2002). For example, *Galium spp.* is typically associated with high vegetative cover of *Carex obnupta*. Clustering compresses hyper-dimensional vegetative data (39 species and bare ground) into a simple association code while retaining underlying relationships in vegetation.

We computed vegetation dissimilarity between data points using a Sørenson (also called *Bray-Curtis*) dissimilarity matrix (Oksanen *et al.,* 2013). Clusters were derived and assigned to data points using a flexible-beta agglomerative hierarchical clustering approach using packages *cluster* and *vegan* in the R statistical environment (Maechler *et al.,* 2013; Oksanen *et al.,* 2013; McCune *et al.,* 2002). We also evaluated Sørenson dissimilarity coupled with the *complete* and *average* clustering method in addition to Euclidean distance coupled with Ward's clustering method (Maechler *et al.,* 2013; Oksanen *et al.,* 2013; McCune *et al.,* 2002).

To evaluate the optimum dendrogram cutoff height, we calculated the average p-value of all species at dendrogram cutoff heights between 0.0 (i.e., every vegetation plot is its own association) to a maximum value of 7.8 (i.e., all vegetation plots belong to the same association) with a step size of 0.01 following the methods of Dufrêne and Legendre (1997). The cutoff height that minimizes the average p-value across all species within the plot is the optimum height. For our dataset, an optimum cutoff of 2.12 yielded 12 vegetation associations.

Our team of Pacific Northwest tidal wetland experts critically reviewed the optimum output of all four clustering strategies. Field experience and professional best judgment of this expert team most approximated the clustering approach created using Sørenson dissimilarity and the flexible-beta linkage, so those methods were selected for our analysis. The other three clustering results significantly differed from our team's judgments and were excluded.

3.3.4 LIDAR Data

We analyzed LIDAR data collected by the Oregon LIDAR Consortium (OLC). OLC is led by the Oregon Department of Geology and Mineral Industries (DOGAMI) and represents a partnership between multiple state and federal agencies. Through coordination and a central responsible agency, OLC collects LIDAR data across much of Oregon using consistent methods and quality assurance procedures. To date, the OLC has acquired more than 69000 km^2 of LIDAR data with a minimum acceptable point density of 8.0 returns$\cdot m^{-2}$ over terrestrial surfaces (DOGAMI, 2013, 2008). The National Science Foundation (NSF) OpenTopography Facility (http://opentopography.org, NSF Award Numbers 0930731 and 0930643) partnered with OLC to disseminate LIDAR point-cloud data. NSF OpenTopography archives all OLC LIDAR point-cloud data, and many other LIDAR datasets across the United States, and makes them available for download using convenient online query tools. NSF OpenTopography delivers the OLC LIDAR data in NAD83 (CORS96) (Epoch 2002) Oregon State Plane Lambert horizontal coordinate system and NAVD88 (GEOID03) vertical datum (Kleber, 2013).

LIDAR data was collected by Watershed Sciences, Inc. for OLC across our study areas. Data was collected during the winter, to minimize the influence of vegetation (Watershed Sciences, Inc. 2009b, 2009c; DOGAMI, 2008). The LIDAR instrument was capable of recording four or more returns per laser pulse (Watershed Sciences, Inc. 2009b, 2009c; DOGAMI, 2008). LIDAR instrument and flight path parameters were structured to provide a minimum illuminated spot size of between 15 cm and 40 cm, laser scan angle of less than ± 15 degrees, and $\geq$ 50% side-lap ($\geq$ 100% overlap) between opposing flight-lines to minimize the influence of laser shadowing and other artifacts (Watershed Sciences, Inc. 2009b, 2009c; DOGAMI, 2008). Aircraft altitude and position were measured by differential survey-grade GPS on-board the aircraft and corrected using a network of survey-grade GPS receivers located at known benchmarks on the ground (Watershed Sciences, Inc. 2009b, 2009c; DOGAMI, 2008). The LIDAR data was processed to align flight-lines, remove pits,

birds, and other artifacts from the data and classify ground points using TerraScan, TerraMatch, and proprietary tools developed by Watershed Sciences prior to delivery to DOGAMI (Watershed Sciences, Inc. 2009b, 2009c; DOGAMI, 2008).

3.3.5 LIDAR-GPS discrepancy

Our objective is to measure the difference between LIDAR-derived DEM elevation and the GPS surveyed marsh surface elevation within common Oregon tidal wetland vegetation communities. Two different approaches are investigated within our research.

First, Watershed Sciences delivered bare-earth digital elevation models to DOGAMI. Raster-based DEMs are typically preferred for GIS purposes because they are more computationally efficient and easier to use than point clouds. Therefore, Oregon LIDAR users will most likely use the raster bare-earth DEM for coastal management objectives. Each vegetation plot data point was assigned an elevation drawn from the spatially-coincident raster cell value of the bare-earth DEM elevation.

Second, past research suggests a minimum-bin gridding technique is capable of mitigating the effect of vegetation (e.g., Ewald, 2013b; Schmid *et al.*, 2011). Minimum-bin techniques search a radius around a given raster cell center for the lowest LIDAR return and assign the elevation of that return to the raster cell value (Ewald, 2013b; Schmid *et al.*, 2011). As the search radius is increased, the probability of capturing a LIDAR return that represents the true ground surface instead of vegetation increases. We assigned the elevation of the lowest LIDAR return within a 1.0 m radius of each vegetation plot center as the minimum-bin LIDAR-derived elevation for that plot. We chose a 1.0 m search radius because the vegetation quadrats that were used to survey vegetation were 1.0 m^2. In addition, the vegetation and topography (e.g., presence of channels) beyond a 1.0 m distance from the plot center was unknown.

The difference between LIDAR-derived elevation and the GPS elevation is the LIDAR-GPS discrepancy, reported in centimeters. Two variants of this metric are

used within our research. The first variant is the difference (D_{BE}, Eq. 3.4) between the bare-earth DEM elevation (H_{BE}) and the GPS surveyed elevation (H_{GPS}).

$$D_{BE} = H_{BE} - H_{GPS} \tag{3.4}$$

The second variant is the difference (D_{MB}, Eq. 3.5) between minimum-bin LIDAR-derived elevation (H_{MB}) and the GPS surveyed elevation (H_{GPS}).

$$D_{MB} = H_{BE} - H_{GPS} \tag{3.5}$$

3.3.6 Statistical Analysis

Our dataset provides statistical challenges because many of our vegetation plots are nested within transects, as well as nested within estuaries. Therefore, each observation is not truly independent of the others, and the potential for spatial autocorrelation between observations of the same species assemblage is high. To address these concerns we employed mixed-effect modeling techniques.

Mixed-effect models (also called *mixed models*) are capable of analyzing uneven and nested sampling designs (Bates, 2010; Zuur *et al.*, 2009, 2007). They grew out of medical and social science fields that required modeling a population-wide response while allowing members of an observational unit (i.e., *level*) within the population to have unit-specific responses (Bates, 2010). For example, every subject in a drug study will respond differently to a dosage of a given drug. Mixed models allow each subject to respond differently to the drug while modeling the population-wide response. In this example, each individual would be a categorical co-variate random-effect and the dosage would be a fixed-effect covariate.

In the context of our research, each vegetation plot was a member of a transect which was nested within an estuary. The unique combinations of transect and estuary are the random effect and the vegetation cluster assignment is the sole fixed effect. LIDAR-GPS discrepancy was the continuous response for our mixed models. If two vegetation plots with the same vegetation association assignment and transect were

observed within the dataset, they were treated as repetitions of the same individual. However, if two vegetation plots had different vegetation associations but shared the same transect they were treated as separate individuals.

We constructed mixed models using package *lme4* (version 1.0-4) in the R statistical environment (Bates *et al.*, 2013; R Development Core Team, 2012). Models were fit using restricted maximum likelihood and Satterthwaite's approximation for degrees of freedom. The vegetation association name was the fixed effect in the mixed model. Two different random-effect structures were evaluated. Model A used only the unique combination of vegetation transect and estuary. The Model B random-effect structure added vegetation percent cover estimating method (i.e., absolute vs. relative). The goal of this model was to test whether our adjustment to relative percent cover (Section 3.2.2) altered our results.

We selected Model B from our two candidate models using Akaike Information Criterion (AIC) and Bayesian Information Criterion (BIC), two model selection metrics rooted in information theory and entropy (Anderson, 2008). AIC and BIC penalize models by the number of parameters they contain. Simple models that accurately model the results are preferred over complex models that slightly improve the model performance (Anderson, 2008). Model selection can be performed by minimizing AIC or BIC across a suite of candidate models (Anderson, 2008). Model B was the simplest model and had a lower AIC and BIC than Model A (Table 3.2). We therefore selected Model B for our analysis. Vegetation associations were statistically compared using multiple comparison contrasts with Tukey-Kramer adjustment, implemented in the R package *multcomp* (Hothorn *et al.*, 2008).

3.4 Results

LIDAR-derived DEM are positively biased across a wide variety of tidal wetland vegetation associations (Figure 3.2, Table 3.3). The LIDAR-GPS discrepancies of all 12 distinct vegetation associations are strongly statistically different from zero (mixed-effect model ANOVA Type III p-value < 0.01). Wet

pasture dominated by slough sedge (*Carex obnupta*, association F) and mid-elevation tidal marsh dominated by Lyngbye's sedge (*Carex lyngbyei*, association H) are statistically different from the other vegetation types but not each other (multiple comparisons with Tukey-Kramer adjustment p-value < 0.05). Vegetation association F is positively biased by a mean LIDAR-GPS discrepancy of 36.6 cm (95% CI: 29.6 cm to 43.6 cm) in the minimum-bin DEM and 39.4 cm (95% CI: 32.2 cm to 46.5 cm) in the DOGAMI bare-earth DEM (Table 3.3, Figure 3.2). Vegetation association H is positively biased by a mean LIDAR-GPS discrepancy of 48.8 cm (95% CI: 40.3 cm to 57.3 cm) in the minimum-bin DEM and 45.1 cm (95% CI: 36.4 cm to 53.8 cm) in the DOGAMI bare-earth DEM.

Low to mid elevation tidal wetland marsh, represented by associations A and G, had the smallest LIDAR-GPS discrepancy and are not statistically different from each other. Vegetation association A (low marsh dominated by tufted hairgrass (*Deschampsia cespitosa*) and low marsh succulents) had a mean positive bias 10.4 cm (95% CI: 5.6 cm to 15.2 cm) in the minimum-bin DEM and 12.3 cm (95% CI: 7.5 cm to 17.2 cm) in the bare-earth DEM. Similarly, vegetation association G (low tidal marsh dominated by seashore saltgrass, *Distichlis spicata*) had a mean minimum-bin LIDAR-GPS discrepancy of 10.6 cm (95% CI: 3.9 cm to 17.3 cm) and the bare-earth DEM had a mean discrepancy of 12.0 cm (95% CI: 5.2 cm to 18.8 cm). Other vegetation types typical of mid to high native tidal marsh and diked pasture have mean LIDAR-GPS discrepancy estimates of between 10 cm and 20 cm. Vegetation associations B, C, D, E, I, J, K, and L are not statistically significantly different from each other (multiple comparisons with Tukey adjustment, p-value > 0.05), although all are statistically different from zero.

Throughout the vegetation types we evaluated, the minimum-bin DEM performs slightly better than the DOGAMI bare-earth DEM. With 95% confidence, the DOGAMI bare-earth DEM elevation is between 2.0 cm and 3.1 cm above the minimum-bin DEM elevation across the entire dataset (mean 2.5 cm, paired two-sided t-test, p-value < 0.001). Mean LIDAR-GPS discrepancy estimates calculated

from the bare-earth DEM and the minimum-bin DEM are statistically different for vegetation associations A, B, D, E, I, J, K, and L (paired two-sided t-test, p-value < 0.05). Vegetation association H differs from the other associations in that the estimated mean minimum-bin LIDAR-GPS discrepancy estimate falls above the mean bare-earth LIDAR-GPS discrepancy estimate. Association H is underrepresented in our dataset with only seven observations. Within association H, the minimum-bin DEM and the bare-earth DEM are not statistically different (two-sided paired t-test p-value: 0.43).

3.5 Discussion

Our results show that LIDAR-derived DEM are positively biased in tidal wetlands. The bare-earth DEM and the minimum-bin filter show similar LIDAR-GPS discrepancy estimates within each vegetation association. *Carex obnupta* and *Carex lyngbyei* wetlands have the largest discrepancy. A large difference between LIDAR-derived estimates of the ground surface and measured GPS elevations is intuitive within these environments because both *Carex obnupta* and *Carex lyngbyei* grow in extremely dense and even stands, often at heights of a meter or more.

Many of our estimates of the difference between LIDAR-derived elevation and GPS-surveyed elevation are similar to past studies in other parts of the world. Schmid *et al.* (2011) found a mean bias of 29.7 cm in *Juncus roemerianus* environments, which is similar to the bias in our *Juncus balticus* mid and high tidal marsh associations (associations C and K, Table 3.3). Our estimates of LIDAR-GPS discrepancy in low tidal marsh with *Salicornia spp*. (association A and G, Table 3.3) are similar to Schmid *et al.* (2011) and Hladik and Alber (2012), who found mean bias of around five to ten centimeters. Sadro *et al.* (2007) found a slightly higher mean discrepancy of 18 cm in *Salicornia spp.* wetlands compared to our estimates. In *Distichlis spicata* wetlands (association G, Table 3.3), we found LIDAR-GPS discrepancy to be significantly less than estimates provided by Hladik and Alber (2012) as well as Sadro *et al.* (2007). Our study adds LIDAR accuracy information

for common tidal wetland and wet pasture communities typical of the Pacific Northwest. As mentioned earlier, *Carex obnupta* and *Carex lyngbyei* wetland vegetation (associations F and H, Table 3.3) have the largest LIDAR-GPS discrepancy within our dataset. In these associations, the range of LIDAR-GPS discrepancy varied from only 3 cm to over 94 cm with mean estimates of 36.6 cm and 48.8 cm, respectively.

LIDAR is an active remote sensing system that relies on the ability of the light pulse to reach the ground. Rosso *et al.* (2006) found that laser pulses were unlikely to penetrate the canopy of *Spartina spp*. Unfortunately, our results show that LIDAR estimates of the ground surface are positively biased even when the minimum-bin technique is used. This suggests that the LIDAR laser pulse never reaches the ground surface within the vegetation communities we studied.

Figure 3.3 provides three examples of LIDAR point-cloud samples within one meter of the GPS measurement. The left panel was collected within a *Carex obnupta* (association F, Table 3.3) stand with vegetation heights of around 1.3 m. The lowest LIDAR return for this area was around 95 cm above the measured ground elevation. The middle panel is a point cloud sample collected in *Carex lyngbyei*. Both *Carex spp.* vegetation types effectively prevent LIDAR from reaching the ground. The far right panel of Figure 3.3 was collected in low tidal marsh dominated by *Deschampsia cespitosa* and succulents (association A, Table 3.3). Minimum-bin LIDAR-GPS discrepancy for this plot was 5.7 cm. Across all three panels, LIDAR penetration to the ground surface appears unlikely. As a result, more advanced filtering procedures are unlikely to improve LIDAR-based estimates of the ground surface elevation because no LIDAR information is available for the filters.

Vegetation will grow to different heights in different locations with varying environmental conditions and stressors (Odum, 1985, 1988; Cornu and Sadro, 2002; Brock and Purkis, 2009). In patchy and disturbed vegetation communities, such as our pasture and restoration site study areas, variability in LIDAR-GPS discrepancy is likely. To be successful, a DEM correction procedure

would need both an accurate high-resolution vegetation map and correction factors specific to the mapped vegetation types. Complex methods, such as those used by Sadro *et al*. (2007), require resources and expertise beyond the scope of most regional and site-specific studies, as well as most on-the-ground restoration efforts.

Variability in LIDAR-GPS discrepancy measurements may also lead to noise in correction factors and may introduce new sources of error into analysis that are not easy to trace. Site specific corrections, such as those applied by past research, may be an appropriate method to develop locally-optimized LIDAR datasets, but ground control and field validation of the corrected DEM is necessary using an independent dataset. In addition, LIDAR-GPS discrepancy is likely a function of the combined effect of multiple layered species. Past research has focused on single-species patches or vegetation associations with low diversity. In situations where multiple species are present, the combined effect of the species together may better predict LIDAR-GPS discrepancy when compared to single species effects. Our clustering approach honors the effect of co-occurring species by compressing the vegetation associates into an association classification. Within our associations, there may be variability in LIDAR-GPS discrepancy that may be possible to explain with statistical models although it would be difficult to identify and model.

In an effort to extract species-specific influences on LIDAR-GPS discrepancy, we built and optimized Boosted Regression Tree (BRT) models following the procedure described by Elith *et al*. (2008). BRTs are a machine-learning technique that builds a series of regression trees and automatically selects variables and interactions that predict the model response (Elith *et al.,* 2008; Hastie *et al.,* 2005). Our BRT models were ultimately abandoned because the results indicated co-linearity between species and did not match field experience. For example, BRT identified *Carex obnupta* and *Galium spp.* as the two most important predictors of LIDAR-GPS discrepancy. In Oregon tidal wetlands, *Galium spp*. often co-occurs with dense *Carex obnupta*. It is likely that *Carex obnupta* is the species that most significantly contributes to LIDAR-GPS discrepancy, not *Galium spp.*; but the co-occurrence of

the two species obscures their contributions. Other species had similar relationships within the BRT model, and we therefore abandoned the BRT approach. Other statistical tools, such as hierarchical partitioning and Bayesian mixture models may provide better results, but the nested structure of our data did not lend itself to those analysis methods (Nally, 1996; Hastie *et al.*, 2005).

3.6 Conclusion

We found that LIDAR-derived digital elevation models are positively biased by vegetation in Oregon tidal wetlands. LIDAR-GPS discrepancy was measured in six Oregon estuaries with twelve common wetland vegetation types, using survey-grade GPS measurements of the marsh plain elevation and LIDAR-derived elevations at the same location. LIDAR estimates of the ground surface in tidal wetlands were typically 10 cm to 30 cm above GPS measurements of the wetland surface. Plant associations dominated by *Carex obnupta* and *Carex lyngbyei* exhibited the largest discrepancy between LIDAR and GPS measurements, with mean discrepancies of 36.6 cm and 48.8 cm respectively. Low tidal marsh associations dominated by a mixture of *Deschampsia cespitosa*, *Distichlis spicata*, *Sarcocornia perennis* and *Jaumea carnosa* had the smallest mean discrepancies of 10 cm to 11 cm. Our research yields new information for coastal LIDAR users and increases our understanding of uncertainty in LIDAR-derived datasets improving our ability to accurately evaluate and effectively manage coastal environments.

3.7 Acknowledgments

This research would not have been possible without the contributions of a variety of partners. GeomaticsResearch provided technical and computing resources. The Marine Resource Management Program at Oregon State University College of Earth, Ocean, and Atmospheric Sciences provided financial and a variety of other assistance. Guidance and mentorship from Jim Graham and Michael Olsen was instrumental in the success of this research.

3.8 Tables and Figures

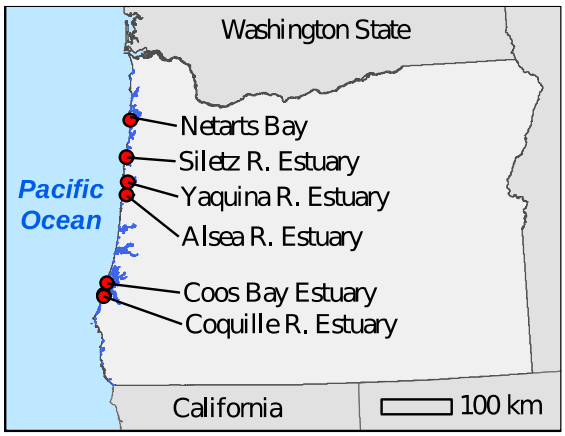

Figure 3.1: Vegetation interference study area. Our dataset consists of 466 locations in six Oregon estuaries from three studies (Janousek and Folger, 2013; Brophy and van de Wetering, 2012; Brophy *et al.*, 2011).

Table 3.1: Estuary data sources. The number of observations (n) and source of data used within this research compiled from three past studies in six estuaries.

Estuary	n	Source
Netarts Bay Estuary	20	Janousek and Folger (2013)
Siletz River Estuary	44	Brophy *et al.* (2011)
Yaquina River Estuary	52	Janousek and Folger (2013)
Alsea River Estuary	17	Janousek and Folger (2013)
Coos Bay Estuary	39	Brophy *et al.* (2011)
Coquille River Estuary	273	Brophy and van de Wetering (2012)
Coquille River Estuary	21	Janousek and Folger (2013)

Table 3.2: Mixed-model performance values for each of the two candidate models. Model A random effect structure included the unique transect-estuary combination and vegetation cover estimation method. Model B included only the unique transect-estuary combination and was selected as the optimum model for our analysis.

Model Name	AIC	BIC	Log-likelihood	Deviance	Rand. Eff.
Model A	3477	3539	-1724	3493	estuaryTransectCombo veg cover method
Model B	3476	3534	- 1724	3492	estuaryTransectCombo

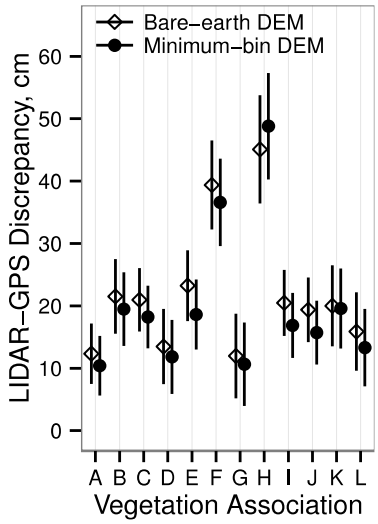

Figure 3.2: Mean LIDAR-GPS discrepancy by vegetation association. Hollow diamonds represent the mean LIDAR-GPS discrepancy for the DOGAMI Bare-earth DEM. Filled circles represent mean LIGAR-GPS discrepancy for the Minimum-bin DEM with a cell size of 1.0 m. Solid vertical lines represent the 95% confidence interval of the estimate.

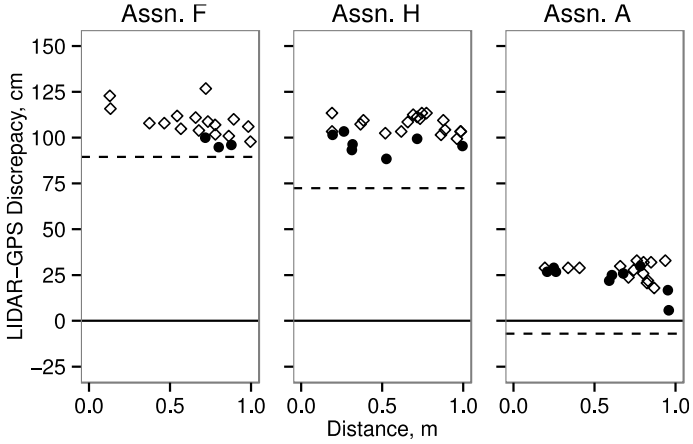

Figure 3.3: Three LIDAR samples within 1.0 m of the GPS point. Hollow diamonds represent unclassified LIDAR returns from the DOGAMI dataset. Filled circles represent ground-classified returns. The dashed line represents the LIDAR-GPS discrepancy of the DOGAMI bare-earth DEM. The left panel is a plot that was assigned to vegetation association F and is dominated by *Carex obnupta*. The middle panel was a sample of vegetation association H and is 40% *Carex lyngbyei*. The right panel is from vegetation association A and has a mix of *Deschampsia cespitosa* and low marsh succulents.

Table 3.3: LIDAR-GPS discrepancy by vegetation association. Mean LIDAR-GPS discrepancy for each of the twelve vegetation associations are reported in centimeters for both the minimum-bin and Bare-earth DEM. All vegetation associations have mean LIDAR-GPS discrepancy estimates that are statistically different from zero (p-value < 0.01).

			Min-bin DEM			Bare-Earth DEM		
Association Description	Name	n	Mean ± SE	Min.	Max.	Mean ± SE	Min.	Max.
Mid-elevation tidal marsh dominated by Lyngbye's sedge (*Carex lyngbyei*)	H	7	48.8 ± 4.4	19.4	88.5	45.1 ± 4.4	14.9	72.6
Wet pasture dominated by slough sedge (*Carex obnupta*)	F	24	36.6 ± 3.6	2.7	94.8	39.4 ± 3.6	-0.9	89.5
Wet pasture dominated by slough sedge (*Carex obnupta*) and water parsley (*Oenanthe sarmentosa*)	B	28	19.5 ± 3.0	-14.4	69.1	21.5 ± 3.0	-15.6	69.0
Moist pasture dominated by Baltic rush (*Juncus balticus*)	K	25	19.6 ± 3.3	6.5	25.6	20.0 ± 3.3	6.1	30.8
High tidal marsh or pasture dominated by Pacific silverweed (*Argentina pacifica*)	E	35	18.6 ± 2.9	-9.9	67.0	23.2 ± 2.9	-2.0	63.8
High tidal marsh dominated by Baltic rush (*Juncus balticus*)	C	53	18.2 ± 2.6	-8.4	45.0	21.0 ± 2.6	-18.2	44.9
Moist pasture dominated by tall fescue (*Festuca arundinacea*)	I	74	16.9 ± 2.7	-3.5	24.9	20.5 ± 2.7	-0.3	38.7
Creeping bentgrass (*Agrostis stolonifera*) wetland	J	39	15.7 ± 2.6	2.0	31.9	19.4 ± 2.6	0.8	52.6
Moist pasture, dominated by a mix of non-native pasture species and Pacific silverweed (*Argentina pacifica*)	L	38	13.3 ± 2.8	5.8	22.0	15.9 ± 3.2	2.3	22.6
Mature high tidal marsh dominated by tufted hairgrass (*Deschampsia cespitosa*)	D	34	11.8 ± 3.0	-18.8	43.0	13.5 ± 3.1	-7.1	49.9
Low tidal marsh dominated by seashore saltgrass (*Distichlis spicata*)	G	23	10.6 ± 3.4	-6.6	21.3	12.0 ± 3.5	-16.7	22.9
Low tidal marsh, dominated by a mix of tufted hairgrass (*Deschampsia cespitosa*) and low marsh succulents	A	84	10.4 ± 2.4	-16.9	57.4	12.3 ± 2.5	-14.8	56.5

4 CONCLUSION

LIDAR-derived DEM are positively biased by tidal wetland vegetation. We found that LIDAR-GPS discrepancy was between 10 cm and 30 cm across a wide range of Oregon tidal wetland communities spanning low to high tidal marsh. Plant associations dominated by *Carex obnupta* and *Carex lyngbyei* exhibited the largest discrepancy between LIDAR and survey-grade GPS measurements. *Carex obnupta* wetlands had a mean LIDAR-GPS discrepancy of 36.6 cm. Mean LIDAR-GPS discrepancy in *Carex lyngbyei* tidal wetlands was 48.8 cm.

The minimum-bin filter technique is capable of partially mitigating vegetation bias within bare-earth DEM. We found an optimum cell size of 1.4 m (1.96 m^2) by evaluating accuracy between cell sizes of 0.1 cm and 6.0 m with a 0.1 m step size in the DEM of a diked tidal wetland restoration site in Oregon. The minimum-bin technique improves DEM performance at cell sizes smaller than the optimum. At cell sizes larger than the optimum, the minimum-bin filter captures and negatively biases the DEM towards channels, ditches, and other low features within the landscape. Our results suggest that minimum-bin techniques may be an appropriate method to generate a locally optimum DEM but should include ground-truthing to validate the results. The optimum cell size will vary by LIDAR collection parameters, return density, ground cover, and topography.

Our research yields new information for coastal LIDAR users and increases understanding of uncertainty in LIDAR-derived datasets, thereby improving the ability to accurately evaluate and effectively manage coastal environments. Future research that evaluates the impact of LIDAR return density on DEM accuracy will further expand understanding of LIDAR error in tidal wetlands. Additional measurements of LIDAR error in tidal wetlands will further refine estimates of LIDAR error by land cover class. However, these estimates will remain sensitive to

the particular type of LIDAR instrument used, flight parameters, seasonal effects, and many other influences.

Applying correction factors to the DEM based on land cover class requires even more complex analysis and introduces new errors into the analysis, further expanding the total error budget. The correction factor technique assumes that LIDAR error is the same in all land covers, similar to the training data, and that the ability to identify land cover is error free. A more defensible approach is to continue research on LIDAR uncertainty in a variety of land cover classes to inform understanding of uncertainty in each of them. We must strive to communicate uncertainty within data products we produce and ask questions that are answerable given the input data.

LIDAR represents one of the most recent advances to drastically shift how we look at and manage the environment. The rapid advancement of sensor technology and the techniques to analyze data will shift how we map and manage the environment into the future. As with all new disruptive technologies, we will continue to learn and refine methods, including both improving sensor capability and understanding of its challenges and errors. LIDAR will not be the last innovation in geospatial science. Therefore, we must carefully examine and quantify uncertainty instead of blindly trusting and extending the technology beyond its capabilities simply because it is exciting and the best available technology.

Coastal zones are challenging to manage because of their complexity, and managers must be comfortable making decisions under conditions of uncertainty. However, the sources and magnitude of that uncertainty must be known and communicated to prevent flawed or incomplete decision-making and inquiry.

BIBLIOGRAPHY

Anderson, D. R. (2008). Model Based Inference in the Life Sciences: A Primer on Evidence. Springer, New York; London.

Athearn, N. D., Takekawa, J. Y., Jaffe, B., Hattenbach, B. J., and Foxgrover, A. C. (2010). Mapping elevations of tidal wetland restoration sites in San Francisco Bay: Comparing accuracy of aerial LIDAR with a singlebeam echosounder. *Journal of Coastal Research*, 26(2):312–319.

Bater, C. W. and Coops, N. C. (2009). Evaluating error associated with LIDAR-derived DEM interpolation. *Computers & Geosciences*, 35(2):289–300.

Bates, D. M., Maechler, M., Bolker, B., and Walker, S. (2013). *lme4: Linear mixed-effects models using Eigen and S4*. R package version 1.0-4.

Bates, D. M. (2010). *lme4: Mixed-effects modeling with R*. Available at http://lme4.r-forge.r-project.org/lMMwR/lrgprt.pdf (accessed December 20, 2013).

Beraldin, J.-A., Blais, F., and Lohr, U. (2010). Laser Scanning Technology. In *Airborne and Terrestrial Laser Scanning*, edited by G. Vosselman and H.G. Maas, pages 1 – 44. Sunbeath, Scotland, UK: Whittles Publishing.

Berber, M., Ustun, A., and Yetkin, M. (2012). Comparison of accuracy of GPS techniques. *Measurement*, 45(7):1742–1746.

Bottom, D. B., Kreag, B., Ratti, F., Roye, C., and Starr, R. (1979). Habitat Classification and Inventory Methods for the Management of Oregon Estuaries. Oregon Department of Fish and Wildlife, Portland, Oregon.

Briese, C. (2010). Extraction of Digital Terrain Models. In *Airborne and Terrestrial Laser Scanning*, edited by G. Vosselman and H.G. Maas, 135–167. Sunbeath, Scotland, UK: Whittles Publishing.

Brock, J. C., and Purkis, S. J. (2009). The Emerging Role of LIDAR Remote Sensing in Coastal Research and Resource Management. *Journal of Coastal Research* 53: 1–5.

Brophy, L., and van de Wetering, S. (2012). Ni-les'tun tidal wetland restoration effectiveness monitoring: Baseline (2010-2011). Technical report, Green Point Consulting, Estuary Technical Group of the Institute for Applied Ecology, and the Confederated Tribes of Siletz Indians, Corvallis, Oregon.

Brophy, L., Cornu, C., Adamus, P., Christy, J., Gray, A., Huang, L., MacClellan, M., Doumbia, J., and Tully, R. (2011). New tools for tidal wetland restoration: development of a reference conditions database and a temperature sensor method for detecting tidal inundation in least-disturbed tidal wetlands of Oregon, USA. Technical report, Cooperative Institute for Coastal and Estuarine Environmental Technology (CICEET), Corvallis, Oregon.

Canty, A. and Ripley, B. D. (2013). *boot: Bootstrap R (S-Plus) Functions.* R package version 1.3-9.

Chassereau, J. E., Bell, J. M., and Torres, R. (2011). A comparison of GPS and LIDAR salt marsh DEMs. *Earth Surface Processes and Landforms*, 36(13):1770–1775.

Chust, G., Galparsoro, I., Borja, A., Franco, J., and Uriarte, A. (2008). Coastal and estuarine habitat mapping, using LIDAR height and intensity and multi-spectral imagery. *Estuarine, Coastal and Shelf Science*, 78(4):633–643.

Cornu, C. E., and Sadro, S. (2002). Physical and functional responses to experimental marsh surface elevation manipulation in Coos Bay's South Slough. *Restoration Ecology*, 10(3):474–486.

Couclelis, H. (2003). The certainty of uncertainty: GIS and the limits of geographic knowledge. *Transactions in GIS*, 7(2):165–175.

Davison, A. C., and Hinkley, D. V. (1997). *Bootstrap Methods and Their Applications*. Cambridge University Press, Cambridge. ISBN 0-521-57391-2.

Diefenderfer, H. L., Coleman, A. M., Borde, A. B., and Sinks, I. A. (2008). Hydraulic geometry and microtopography of tidal freshwater forested wetlands and implications for restoration, Columbia River, U.S.A. *Ecohydrology and Hydrobiology*, 8(2):339–361.

DOGAMI (2013). DOGAMI fact sheet: LIDAR data acquisition, uses, & partners. Technical Report, Oregon Department of Geology and Mineral Industries (DOGAMI), Oregon LIDAR Consortium. Available at http://www.oregongeology.org/pubs/fs/lidar-leg-fact-sheet.pdf (accessed December 20, 2013).

DOGAMI (2009). OLC South Coast Delivery 5 Acceptance Report. Technical Report. Oregon Department of Geology and Mineral Industries (DOGAMI), Oregon LIDAR Consortium. Portland, Oregon.

DOGAMI (2008). Oregon LIDAR Consortium: LIDAR specifications. Technical Report. Oregon Department of Geology and Mineral Industries (DOGAMI), Oregon LIDAR Consortium. Portland, Oregon. Available at http://www.oregongeology.org/sub/projects/olc/olc_lidar_spec.pdf (accessed December 20, 2013).

Ducks Unlimited. (2010). Ni-les'tun Unit restoration: USFWS Bandon Marsh National Wildlife Refuge design. Designed by Randy Van Hoy, Surveyed by Pat Schulte.

Dufrêne, M. and Legendre, P. (1997). Species Assemblages and Indicator Species: The Need for a Flexible Asymmetrical Approach. *Ecological Monographs*, 67(3):345–366.

Elith, J., Leathwick, J. R., and Hastie, T. (2008). A working guide to boosted regression trees. *Journal of Animal Ecology*, 77(4):802–13.

Elliott, M., and Whitfield, A. K. (2011). Challenging paradigms in estuarine ecology and management. *Estuarine, Coastal and Shelf Science*, 94(4):306–314.

Engle, V., Kurtz, J., Smith, L., Chancy, C., and Bourgeois, P. (2007). A classification of U.S. estuaries based on physical and hydrologic attributes. *Environmental Monitoring and Assessment*, 129(1):397–412.

Ewald, M. J. (2013a). Ni-les'tun Unit of the Bandon Marsh National Wildlife Refuge tidal datums. Unpublished data.

Ewald, M. J. (2013b). LIDAR in coastal wetlands: selecting the optimum cell size for a minimum-bin digital elevation model. In Preparation.

Ewald, M. J., and Brophy, L. S. (2012). Tidal Wetland Prioritization for the Tillamook Bay Estuary. Prepared for the Tillamook Estuaries Partnership, Garibaldi, Oregon. Green Point Consulting, Corvallis, Oregon.

Frenkel, R., Eilers, H., and Jefferson, C. (1981). Oregon coastal salt marsh upper limits and tidal datums. *Estuaries and Coasts*, 4(3):198–205.

Guichard, F. and Peterson, G. (2009). Ecological Cross-Scale Interactions. In *Ecosystem-Based Management for the Oceans*, edited by K. McLeod and H. Leslie, pages 74–91. Island Press, Washington, DC.

Hawes, S., Hiebler, J., Nielsen, E., Alton, C., Christy, J., and Benner, P. (2008). Historical vegetation of the Pacific Coast, Oregon, 1855-1910. ESRI ArcMap ShapeFile, Version 2008_03, Available at http://www.pdx.edu/pnwlamp/historical-vegetation-maps-for-pacific-northwest (accessed December 20, 2013).

Hastie, T., Tibshirani, R., and Friedman, J. (2005). The Elements of Statistical Learning: Data Mining, Inference and Prediction. Springer Series in Statistics. Second Edition. Springer, New York.

Hladik, C. and Alber, M. (2012). Accuracy assessment and correction of a LIDAR-derived salt marsh digital elevation model. *Remote Sensing of Environment*, 121:224–235.

Hodgson, M. E. and Bresnahan, P. (2004). Accuracy of airborne LIDAR-derived elevation: empirical assessment and error budget. *Photogrammetric Engineering and Remote Sensing*, 70(3):331–340.

Hothorn, T., Bretz, F., and Westfall, P. (2008). Simultaneous inference in general parametric models. *Biometrical Journal*, 50(3):346–363.

Janousek, C. N. and Folger, C. L. (2013). Variation in tidal wetland plant diversity and composition within and among coastal estuaries: assessing the relative importance of environmental gradients. *Journal of Vegetation Science*. In Press.

Jefferson, C.A. (1975). Plant communities and succession in Oregon coastal salt marshes. Ph.D. Thesis, Department of Botany and Plant Pathology, Oregon State University.

Kentula, M. E. (2000). Perspectives on setting success criteria for wetland restoration. *Ecological Engineering*, 15(3–4):199 – 209.

Kleber, E. (2013). National Science Foundation OpenTopography Facility. Personal communication. January 18, 2013.

Lee, H. II, Reusser, D.A., Haggerty, P., Brown, C.A., and Clinton, P.J. (2009). Regional classification of Pacific Northwest estuaries by wetland and land cover patterns. Chapter 2 in: *Classification of regional patterns of environmental drivers and benthic habitats in Pacific Northwest estuaries*. H. Lee II and C.A. Brown (Eds.). U.S. EPA, Office of Research and Development, National Health and Environmental Effects Research Laboratory, Western Ecology Division. EPA/600/R-09/140.

Lohani, B., and Mason, D. C. (2001). Application of airborne scanning laser altimetry to the study of tidal channel geomorphology. *ISPRS Journal of Photogrammetry and Remote Sensing*, 56(2):100–120.

Maechler, M., Rousseeuw, P., Struyf, A., Hubert, M., and Hornik, K. (2013). *cluster: Cluster Analysis Basics and Extensions*. R package version 1.14.4.

McCune, B., Grace, J. B., and Urban, D. L. (2002). *Analysis of Ecological Communities*. MjM Software Design. Gleneden Beach, Oregon.

McLeod, K. and Leslie, H. (2009). Ecosystem-Based Management for the Oceans. Island Press, Washington, DC.

Meng, X., Currit, N., and Zhao, K. (2010). Ground filtering algorithms for airborne LIDAR data: A review of critical issues. *Remote Sensing*, 2(3):833–860.

Moeslund, J. E., Arge, L., BØcher, P. K., Nygaard, B., and Svenning, J. C. (2011). Geographically comprehensive assessment of salt-meadow vegetation-elevation relations using LIDAR. *Wetlands*, 31(3):471–482.

Montané, J. M. and Torres, R. (2006). Accuracy assessment of LIDAR saltmarsh topographic data using RTK GPS. *Photogrammetric Engineering and Remote Sensing*, 72(8):961–967.

Nally, R. M. (1996). Hierarchical partitioning as an interpretative tool in multivariate inference. *Austral Ecology*, 21(2):224–228.

Odum, E. P. (1985). Trends Expected in Stressed Ecosystems. *BioScience*, 35(7):419-422.

Odum, E. P. (1988). Comparative Ecology of Tidal Freshwater and Salt Marshes. *Annual Review of Ecology and Systematics*, 19:147-176.

Oksanen, J., Blanchet, F. G., Kindt, R., Legendre, P., Minchin, P. R., O'Hara, R. B., Simpson, G. L., Solymos, P., Stevens, M. H. H., and Wagner, H. (2013). *vegan: Community Ecology Package*. R package version 2.0-9.

Palmer, M. (2009). Reforming watershed restoration: Science in need of application and applications in need of science. *Estuaries and Coasts*, 32(1):1–17.

Pebesma, E. J. (2004). Multivariable geostatistics in s: the gstat package. *Computers & Geosciences*, 30:683–691.

Poulter, B. and Halpin, P. N. (2008). Raster modelling of coastal flooding from sea-level rise. *International Journal of Geographical Information Science*, 22(2):167–182.

R Core Team (2012). *R: A Language and Environment for Statistical Computing*. R Foundation for Statistical Computing, Vienna, Austria. ISBN 3-900051-07-0.

Ricketts, P. J. (1992). Current approaches in geographic information systems for coastal management. *Marine Pollution Bulletin*, 25(1–4):82 – 87.

Rosenberg, A. A., and Sandifer, P. A. (2009). What do managers need? In *Ecosystem-Based Management for the Oceans*, edited by K. McLeod and H. Leslie, pages 13–30. Island Press, Washington, DC.

Rosso, P. H., Ustin, S. L., and Hastings, A. (2006). Use of LIDAR to study changes associated with Spartina invasion in San Francisco Bay Marshes. *Remote Sensing of Environment*, 100(3):295–306.

Sadro, S., Gastil-Buhl, M., and Melack, J. (2007). Characterizing patterns of plant distribution in a southern California salt marsh using remotely sensed topographic and hyperspectral data and local tidal fluctuations. *Remote Sensing of Environment*, 110(2):226 – 239.

Schmid, K. A., Hadley, B. C., and Wijekoon, N. (2011). Vertical accuracy and use of topographic LIDAR data in coastal marshes. *Journal of Coastal Research*, 27(6A):116–132.

Schulte, P. (2013). Ducks Unlimited. Personal communication. January 13, 2013.

Seliskar, D.M., and Gallagher, J.L. (1983). The ecology of tidal marshes of the Pacific Northwest coast: A community profile. U.S. Fish and Wildlife Service, Division of Biological Services, Washington, D.C. FWS/OBS-82/32.

Shackeroff, J. M., Hazen, E. L., and Crowder, L. B. (2009). The Oceans as Peopled Seascapes. In *Ecosystem-Based Management for the Oceans*, edited by K. McLeod and H. Leslie, pages 33–54. Island Press, Washington, DC.

Simenstad, C., Tanner, C., Grandell, C., White, J., and Cordell, J. K. J. (2005). Challenges of habitat restoration in a heavily urbanized estuary: Evaluating the investment. *Journal of Coastal Research*, 40:6–23.

Wang, C., Menenti, M., Stoll, M. P., Feola, A., Belluco, E., and Marani, M. (2009). Separation of ground and low vegetation signatures in LIDAR measurements of salt-marsh environments. *Geoscience and Remote Sensing, IEEE Transactions on*, 47(7):2014–2023.

Watershed Sciences, Inc. (2009a). LIDAR Remote Sensing Data Collection: DOGAMI, Southern Oregon Coast Study Area – Delivery 5. Technical Report. Submitted to Oregon Department of Geology and Mineral Industries (DOGAMI).

Watershed Sciences, Inc. (2009b). LIDAR Remote Sensing Data Collection: DOGAMI, South Oregon Coast Study Area. Technical Report. Submitted to Oregon Department of Geology and Mineral Industries (DOGAMI). Available at http://www.oregongeology.org/sub/projects/olc/watershedsci/South_Coast_Lidar_Report_2008.pdf (accessed December 20, 2013).

Watershed Sciences, Inc. (2009c). LIDAR Remote Sensing Data Collection: DOGAMI, Oregon North Coast Study Area. Technical Report. Submitted to Oregon Department of Geology and Mineral Industries (DOGAMI). Available at http://www.oregongeology.org/sub/projects/olc/watershedsci/North_Coast_Lidar_Report_2009.pdf (accessed December 20, 2013).

Wehr, A. and Lohr, U. (1999). Airborne laser scanning—an introduction and overview. *ISPRS Journal of Photogrammetry and Remote Sensing*, 54(2–3):68–82.

Willmott, C. J. and Matsuura, K. (2005). Advantages of the mean absolute error (MAE) over the root mean square error (RMSE) in assessing average model performance. *Climate Research*, 30:79–82.

Zuur, A. F., Ieno, E. N., and Smith, G. M. (2007). *Analyzing Ecological Data*. Springer, New York, NY.

Zuur, A. F., Ieno, E. N., Walker, N., Saveliev, A. A., and Smith, G. M. (2009). *Mixed effects models and extensions in ecology with R*. Springer, New York, NY.

APPENDICES

APPENDIX A

Species Present Within the Study Plots

APPENDIX A SPECIES PRESENT WITHIN THE STUDY PLOTS

Table A.1. Tidal wetland species scientific name, six-letter abbreviation, and number of observations within the dataset. Number of observations are not exclusive, and multiple species can be present within a single vegetation plot.

	Name	n		Name	n
1	*Agrostis spp.* (AGRspp)	299	21	*Trifolium wormskioldii* (TRIWOR)	36
2	*Juncus balticus* (JUNBAL)	239	22	*Trifolium repens* (TRIREP)	30
3	*Potentilla anserina* (POTANS)	182	23	*Oenanthe sarmentosa* (OENSAR)	27
4	*Deschampsia cespitosa* (DESCES)	163	24	*Grindelia stricta* (GRISTR)	26
5	*Distichlis spicata* (DISSPI)	156	25	*Juncus effusus* (JUNEFF)	23
6	*Sarcocornia perennis* (SARPER)	152	26	*Plantago spp.* (PLAspp)	22
7	*Jaumea carnosa* (JAUCAR)	151	27	*Hypochaeris radicata* (HYPRAD)	22
8	*Schedonorus arundinaceus* (SCHARU)	132	28	*Achillea millefolium* (ACHMIL)	22
9	*Triglochin maritima* (TRIMAR)	125	29	*Rumex spp.* (RUMspp)	20
10	*Lotus corniculatus* (LOTCOR)	116	30	*Phalaris arundinacea* (PHAARU)	20
11	*Holcus lanatus* (HOLLAN)	116	31	*Vicia nigricans ssp. gigantea* (VICNIG)	19
12	*Carex lyngbyei* (CARLYN)	92	32	*Spergularia spp.* (SPEspp)	19
13	*Glaux maritima* (GLAMAR)	74	33	*Festuca rubra* (FESRUB)	17
14	*Atriplex patula* (ATRPAT)	73	34	*Alopecurus pratensis* (ALOPRA)	14
15	*Hordeum spp.* (HORspp)	65	35	*Alopecurus geniculatus* (ALOGEN)	14
16	*Carex obnupta* (CAROBN)	54	36	*Castilleja ambigua* (CASAMB)	13
17	*Cuscuta pacifica* (CUSPAC)	53	37	*Typha latifolia* (TYPLAT)	12
18	*Symphyotrichum subspicatum* (SYMSUB)	47	38	*Angelica lucida* (ANGLUC)	11
19	*Galium spp.* (GALspp)	47	39	*Juncus bufonius* (JUNBUF)	10
20	*Eleocharis palustris* (ELEPAL)	38			

APPENDIX B

Glossary

APPENDIX B GLOSSARY

Absolute Percent Cover	The percentage of a one square meter quadrat covered by a given species, reported as a percentage and *including* layering within a plot; calculated total (sum) cover by all species in a plot may exceed 100%; see Section 3.3.2.1
Accuracy	A metric used to describe the difference between a known value and a measured value; differs from *precision*
Pasture	An agricultural field primarily used to raise livestock, often with vegetation species planted for that purpose
AIC	Akaike Information Criterion; a model selection metric based in Information Theory; see Anderson (2008)
Airborne LIDAR	A LIDAR system flown onboard an aircraft such as a fixed-wing airplane or helicopter
Bare-earth DEM	A DEM digitally removed of trees, buildings, and other objects that fall above the ground surface; see DEM
BIC	Bayesian Information Criterion; a model selection metric based in Information Theory; see Anderson (2008)
Cell size	The geographic length of one side of a raster cell
Channel	A depression in the landscape, sometimes constructed, that conveys water
CORS96	An adjustment to the North American Datum of 1983 (NAD83)
Datum	The specifications of a measurement system, to which measurements can be referenced and communicated (e.g., *NAVD88* and *MHHW*)
DEM	Digital Elevation Model; a digital representation of terrain; usually in a raster data model referenced to a common datum for the purposes of describing topographic relief
Differential GPS	A technique that requires two or more GPS receivers to provide position correction factors from a stationary reference receiver at a known location to a roving GPS receiver
Dike	A constructed berm to restrict or prevent water from entering an area
Ditch	A constructed water conveyance structure, often designed to rapidly drain frequently inundated land (e.g., an agricultural field)

DOGAMI	Oregon Department of Geology and Mineral Industries
EBM	Ecosystem Based Management; see McLeod and Leslie (2009)
EPSG	A code used to reference a standardized geographic coordinate system, datum, or coordinate transformation to the Geodetic Parameter Registry provided by the European Petroleum Survey Group
Error	The difference between a measured value and the true value, considering both *accuracy* and *precision*
Geoid	The shape the oceans would take if they covered the Earth, absent of land, and subjected only to the gravitational forces and rotation
GEOID03	A model of the geoid published by NOAA National Geodetic Survey and used to compute NAVD88 orthometric heights
GPS	Global Positioning System
High marsh	Tidal marshes that lie high within the tide frame (usually 40 cm or greater above mudflat), above low and mid marsh; typically peat over silt substrate; see Seliskar and Gallagher (1983)
HMT	Highest Measured Tide; the highest tide recorded at a location
LIDAR	Light Detection and Ranging; a remote sensing technique that uses an active laser to measure the distance from the sensor to the target.
Least-disturbed wetland	A wetland, free of major alterations and typically vegetated with species adapted to the hydrologic and environmental conditions of the site
LIDAR pulse	The burst of energy emitted from the laser of a LIDAR instrument
Low marsh	A wetland located low in the tide frame slightly above mudflat; typically clay or sand substrate; see Seliskar and Gallagher (1983)
MAE	Mean Absolute Error; see Section 2.3.4
MHHW	Mean Higher High Water; a tidal datum; the mean elevation of the higher high water peak of each tidal day over the National Tidal Datum Epoch
Mid marsh	A transitional wetland between low and high marsh; with a silty substrate; see Seliskar and Gallagher (1983)
Minimum-bin DEM	A digital elevation model created by assigning the elevation of the lowest LIDAR return within a given raster cell or search radius of a pixel center
MLLW	Mean Lower Low Water; a tidal datum; the mean elevation of the lower low water trough of each tidal day over the National Tidal Datum Epoch
MSP	Marine Spatial Planning; see McLeod and Leslie (2009)

NAD83	North American Datum of 1983; a standardized horizontal coordinate system and datum for North America
Native wetland	A wetland, typically undisturbed, with vegetation species indigenous to the region and adapted to site-specific environmental conditions
Natural levee	A natural berm, typically formed by fluvial deposition of sediment onto a river bank during flooding conditions.
NAVD88	North American Vertical Datum of 1988; a standardized orthometric vertical datum for North America
NGS	NOAA National Geodetic Survey
NOAA	National Oceanic and Atmospheric Association
OLC	Oregon LIDAR Consortium; a collection of state and federal agencies that coordinate, acquire, and disseminate LIDAR data within Oregon
Orthometric height	The vertical distance from a location to the geoid
Pacific Northwest	An ecoregion in the United States and Canada; consisting of Oregon, Washington, Idaho, and British Columbia; typically west of the Cascade Mountain range but including the Columbia River watershed
Precision	A measure of random error in a estimated value; the degree of closeness from one repeated measurements suite of a value to another set of repeated measurements of the same quantity
Pulse return density	The number of LIDAR measurements within a given ground region divided by the area of that region
Raster	A dot matrix data model that encodes data into a rectangular grid of equal size pixels. Pixels are usually square.
Relative Percent Cover	The percentage of a one square meter quadrat covered by a given species, reported as a percentage and *excluding* layering within a plot; calculated total (sum) cover by all species in a plot may *not* exceed 100%; see Section 3.3.2.1
Restoration	A management intervention designed to return the environmental conditions and processes to a natural state that existed before disturbance
RMSE	Root Mean Square Error; see Section 2.3.4
Species assemblage	A community of co-occurring species; also see *vegetation association*
Spot diameter	The illuminated ground area from a LIDAR pulse

Tidal datum	A vertical datum that is referenced against a defined phase of the tide such as Mean Higher High Water (MHHW).
Tidal wetland	A wetland inundated by the tides at least once a year.
Tide gate	A water control structure designed to prevent water from entering an area (e.g. agricultural field) on a rising tide but allow water to exit the area during a falling tide or during periods of flooding
Uncertainty	The degree of confidence in an estimate of the difference between an estimated and true value; differs from *accuracy* and *precision*
UTM	Universal Transverse Mercator; a projected horizontal coordinate system with sixty zones covering the surface of the Earth. Each zone is individually projected using a secant transverse Mercator projection.
Vegetation association	A community of plant species that typically co-occur on the landscape; also see *species assemblage*
Wetland	Land area where soil development, vegetation communities, and environmental conditions reflect water-saturated soil; soil surface may be periodically inundated with water

APPENDIX C

Vegetation Species Diagnostic Plotting

APPENDIX C VEGETATION SPECIES DIAGNOSTIC PLOTTING

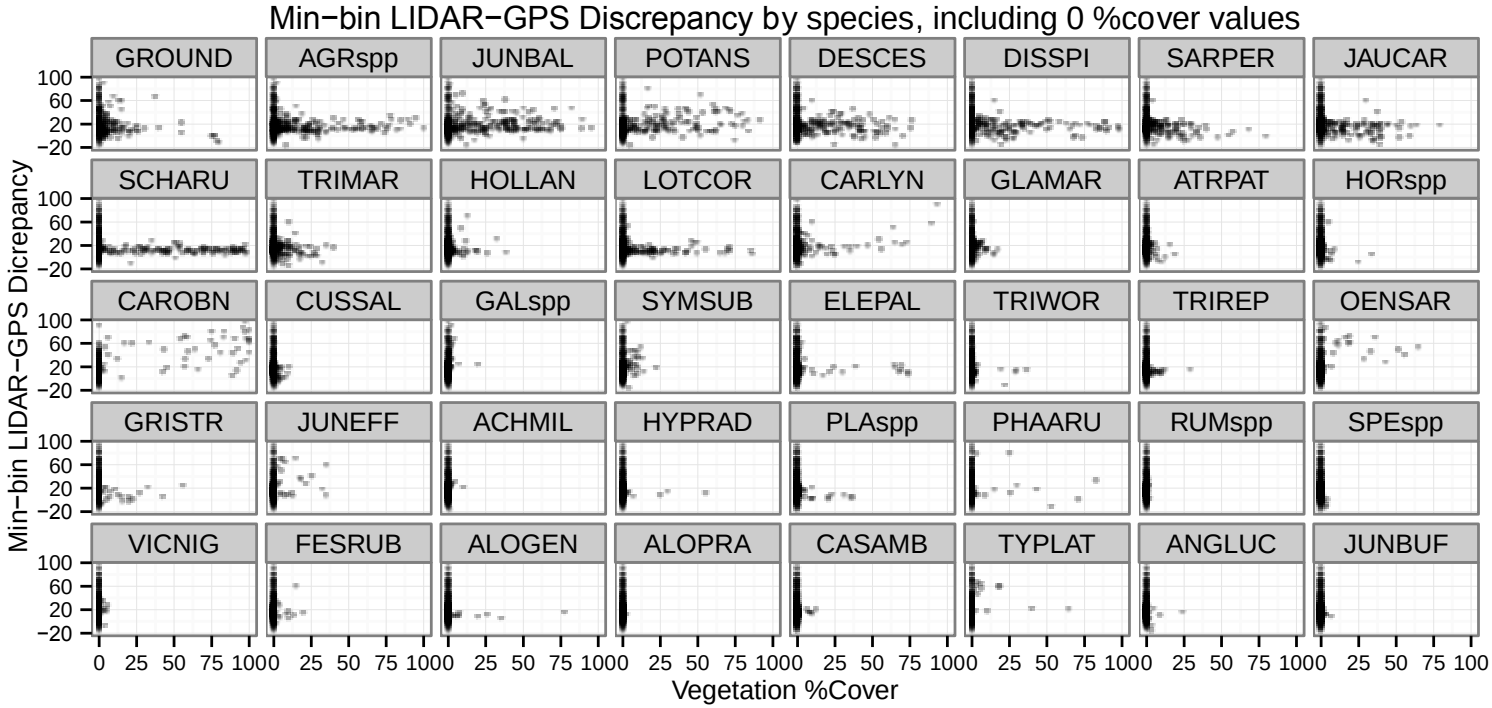

Figure C.1. Minimum-bin LIDAR-GPS discrepancy scatter plots faceted by species, *including* zero percent cover data points. Refer to Table A.1 to associate six-letter species codes to each species.

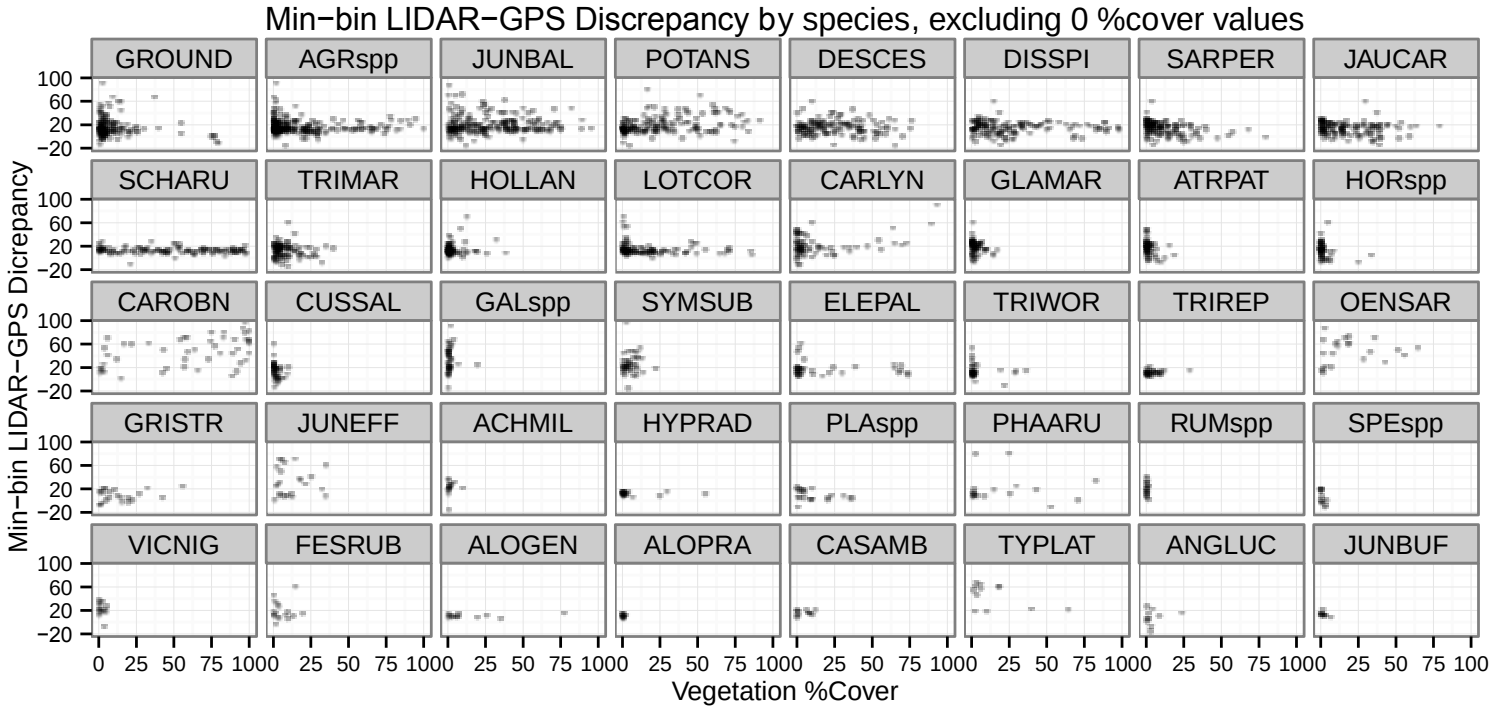

Figure C.2. Minimum-bin LIDAR-GPS discrepancy scatter plots faceted by species, *excluding* zero percent cover data points. Refer to Table A.1 to associate six-letter species codes to each species.

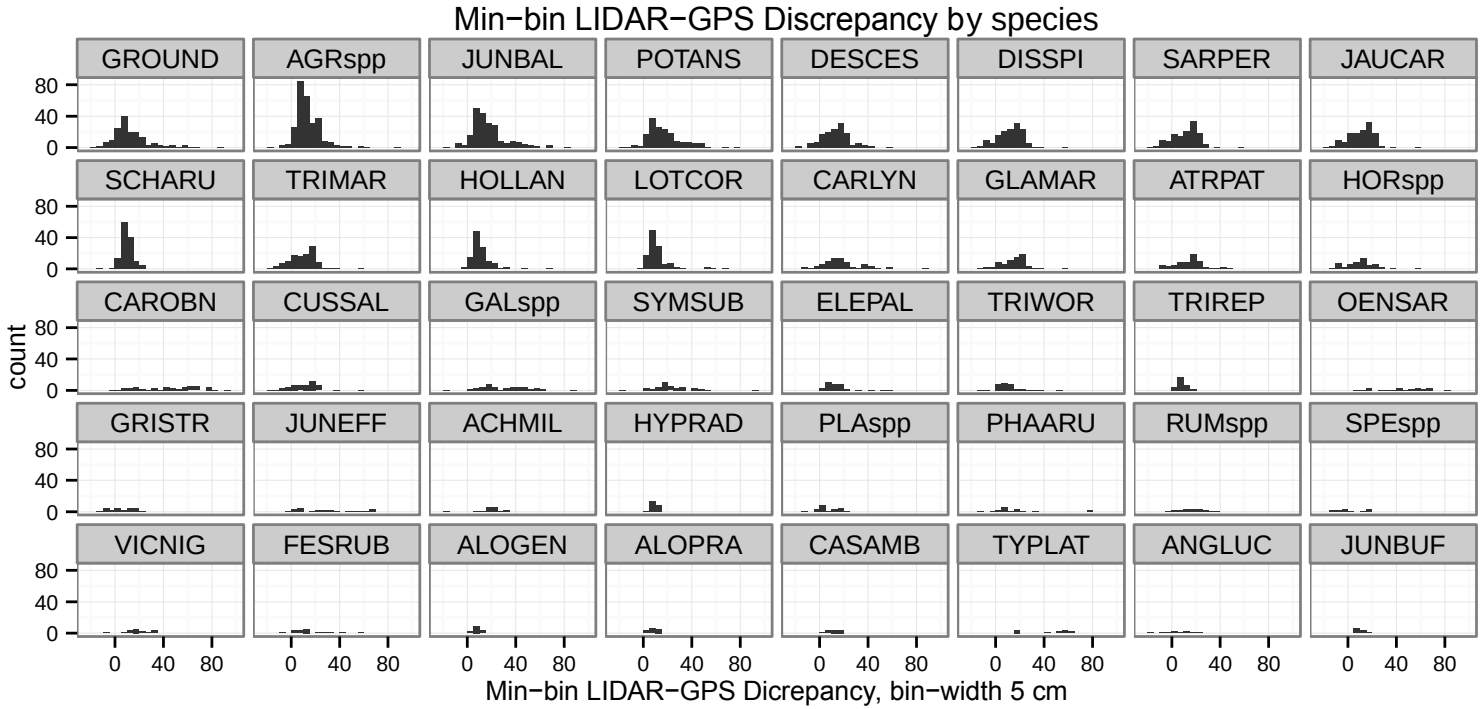

Figure C.3. Minimum-bin LIDAR-GPS discrepancy histogram plots faceted by species, *excluding* zero percent cover data points. Refer to Table A.1 to associate six-letter species codes to each species.

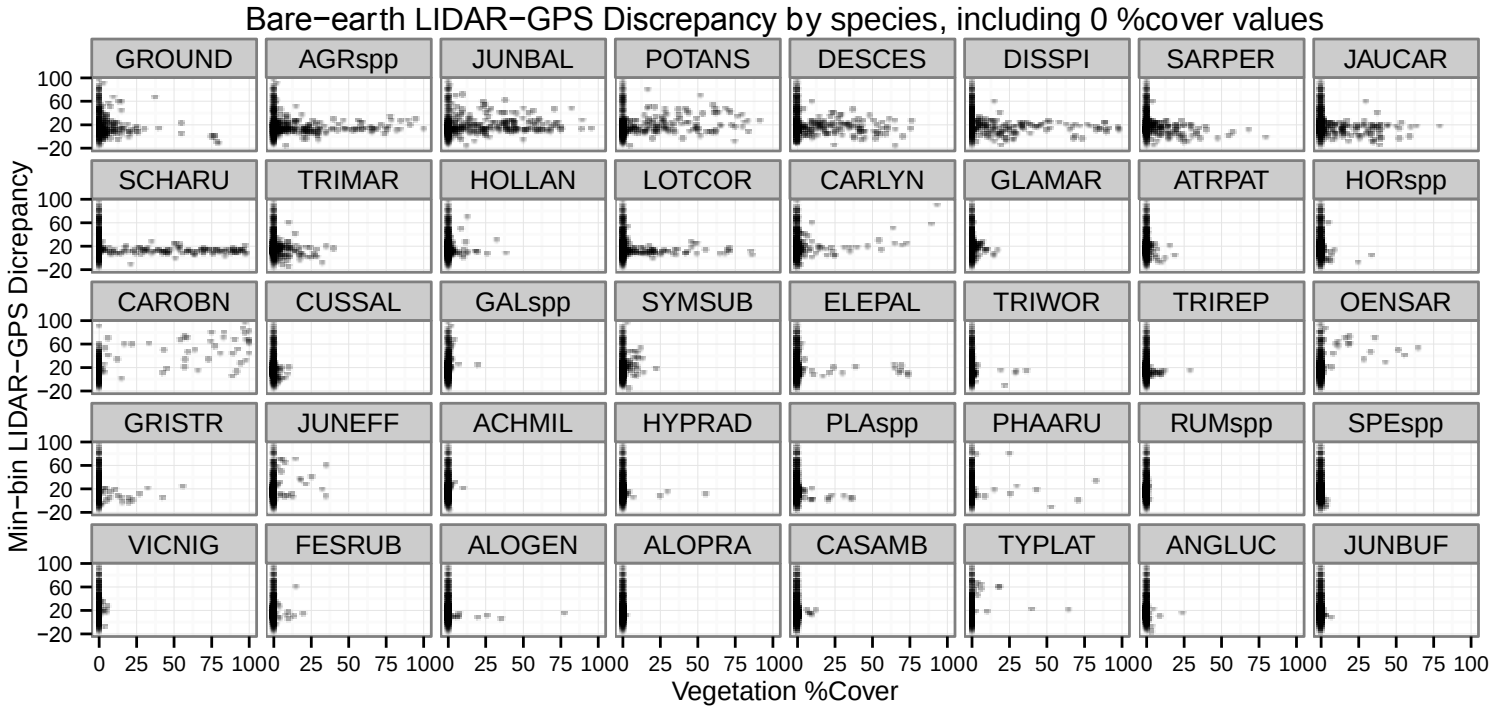

Figure C.4. DOGAMI bare-earth LIDAR-GPS discrepancy scatter plots faceted by species, *including* zero percent cover data points. Refer to Table A.1 to associate six-letter species codes to each species.

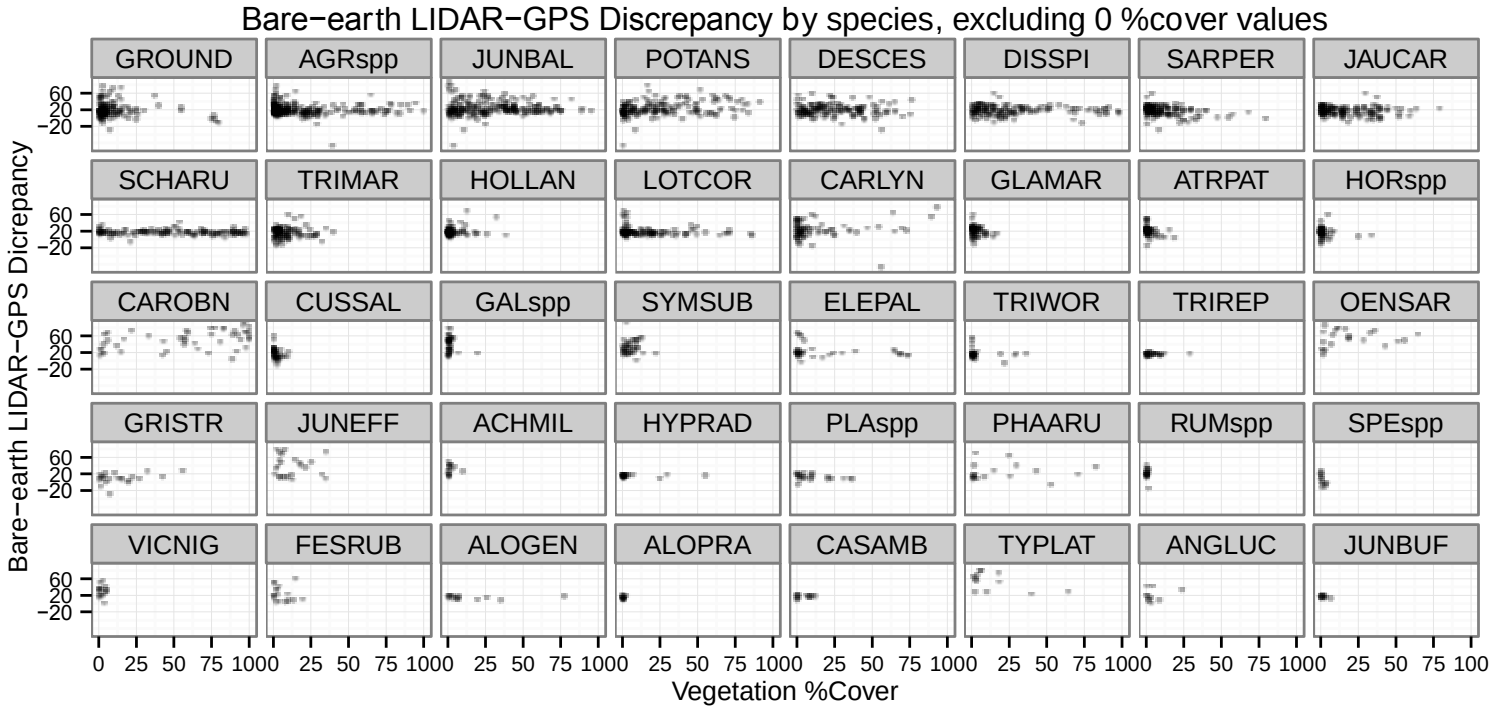

Figure C.5. DOGAMI bare-earth LIDAR-GPS discrepancy scatter plots faceted by species, *excluding* zero percent cover data points. Refer to Table A.1 to associate six-letter species codes to each species.

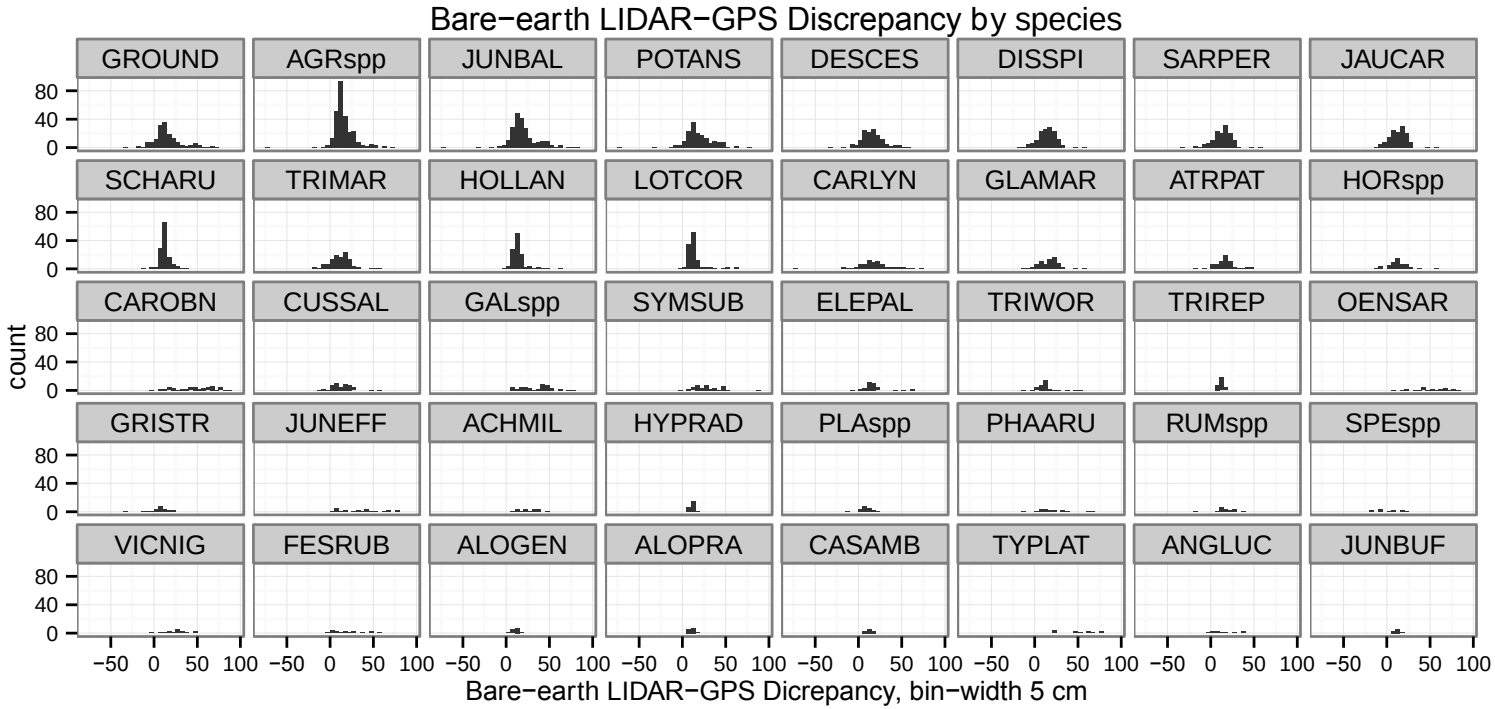

Figure C.6. DOGAMI bare-earth LIDAR-GPS discrepancy histogram plots faceted by species, *excluding* zero percent cover data points. Refer to Table A.1 to associate six-letter species codes to each species.

APPENDIX D

Quantitative Clustering of Vegetation Data

APPENDIX D QUANTITATIVE CLUSTERING OF VEGETATION DATA

The figures and tables in this appendix support the quantitative vegetation data clustering approach used within this thesis. Clustering involves many decisions including the type of clustering method and where to break the resulting dendrogram to form the clusters. Although the hope is that the final cluster assignments reflect the trends within the data, one critique of clustering techniques has been that they are somewhat arbitrary. Rather than making arbitrary decisions, we followed the methods proposed by Dufrêne and Legendre (1997) to break the dendrogram by minimizing the average p-value across all species. We computed the full Indicator Species Analysis suite of cluster performance metrics across the full range of dendrogram heights with a 0.01 step size. Figure D.1 plots these metrics. Figure D.2 plots the mean percent cover of each tidal wetland species within each cluster assignment. Table A.1 relates the species number along the X axis of Figure D.2 to its name.

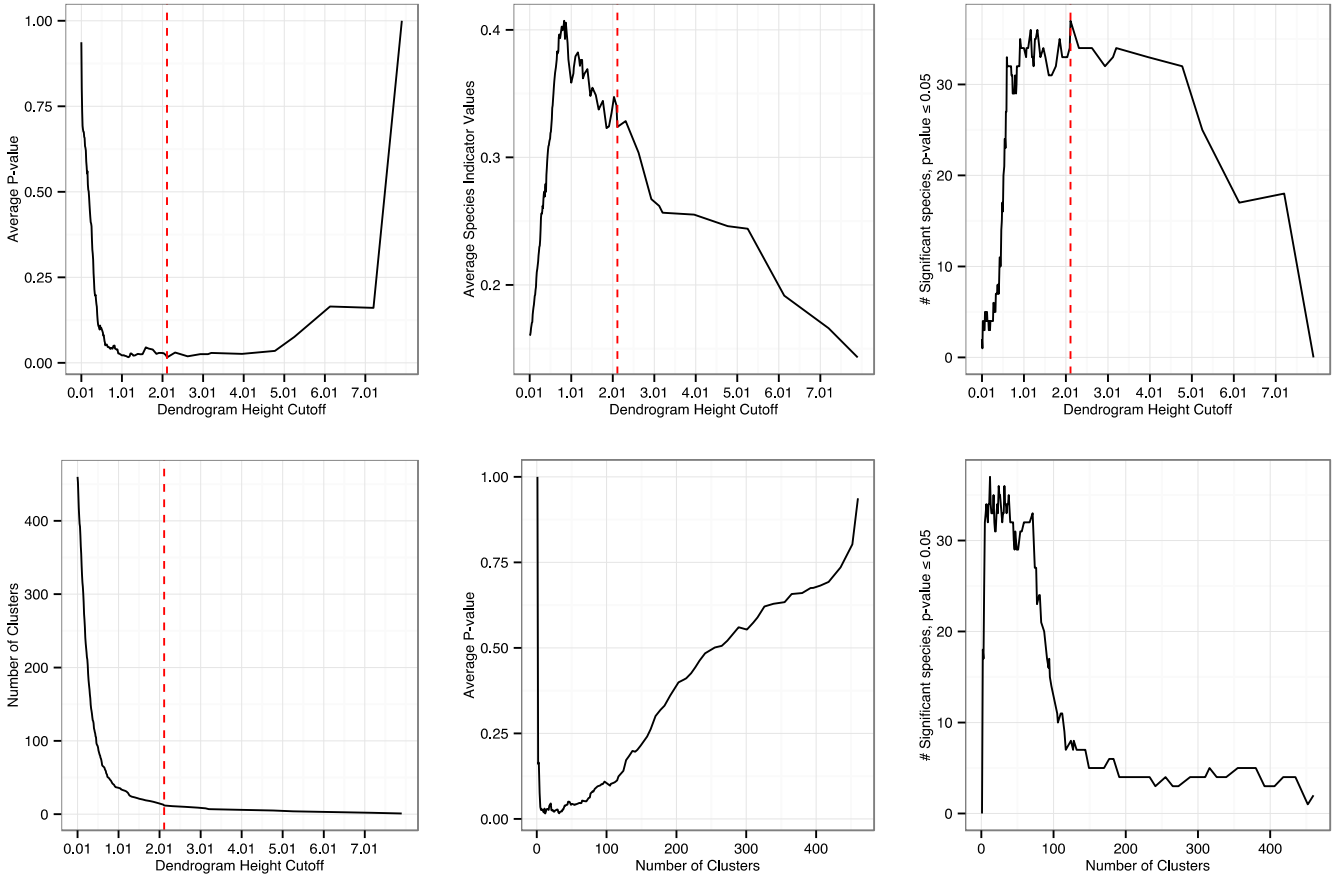

Figure D.1. Dendrogram cutoff height calibration plots. The dashed red line represents the selected cutoff height.

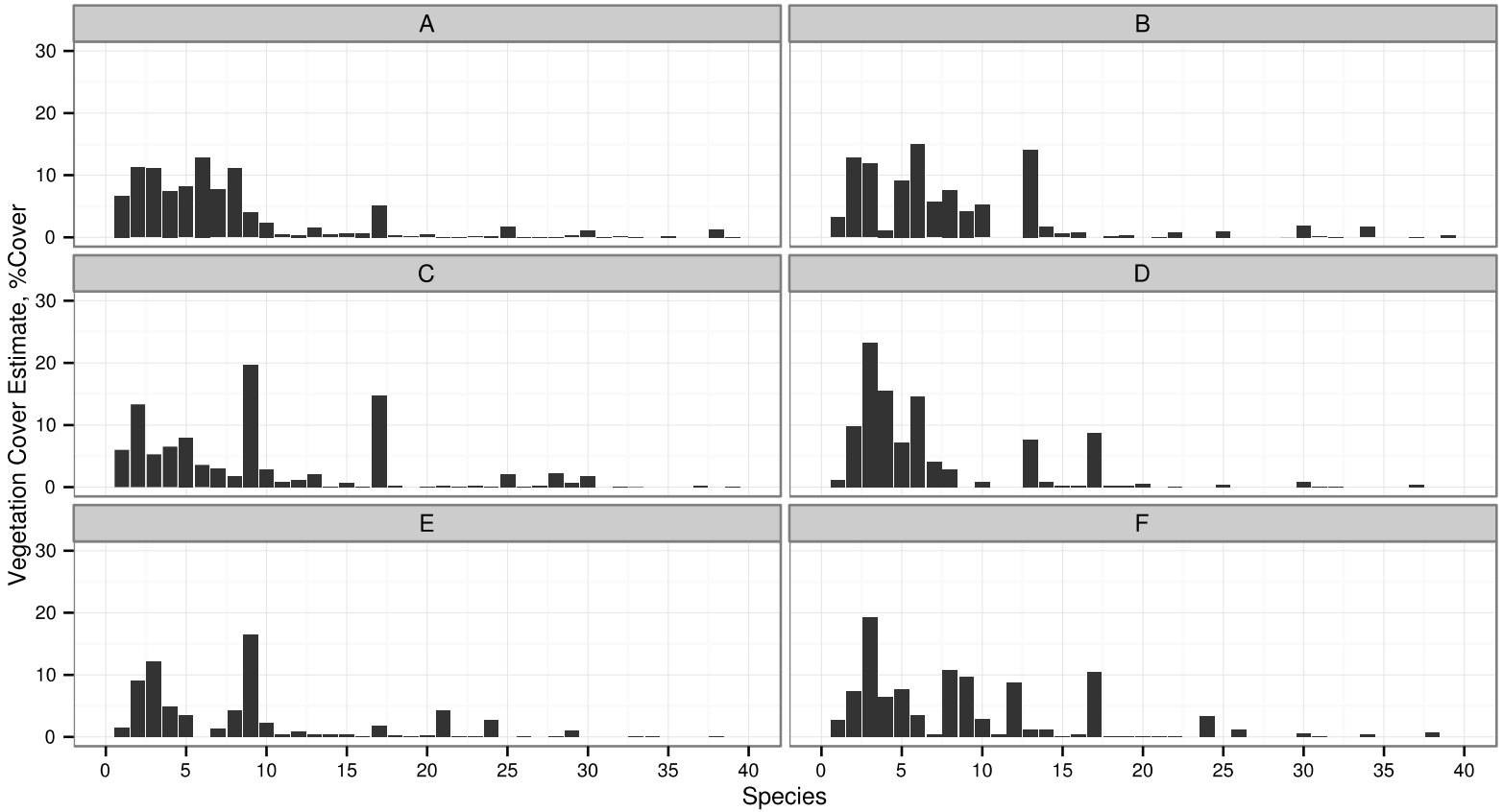

Figure D.2. Mean percent cover of each species faceted by vegetation association cluster assignment. Relate species number to species name using Table A.1.

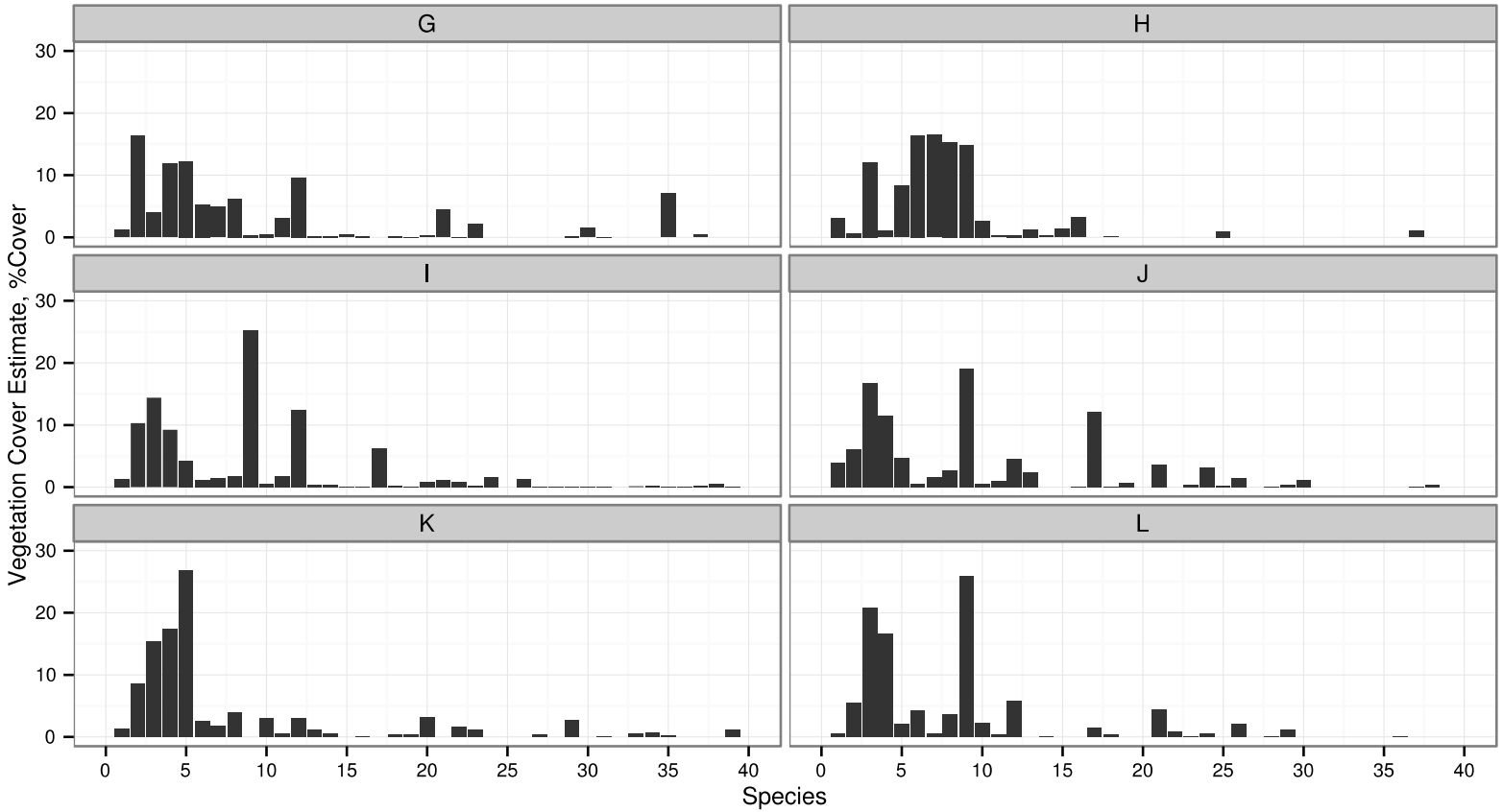

Figure D.2 (continued). Mean percent cover of each species faceted by vegetation association cluster assignment. Relate species number to species name using Table A.1.

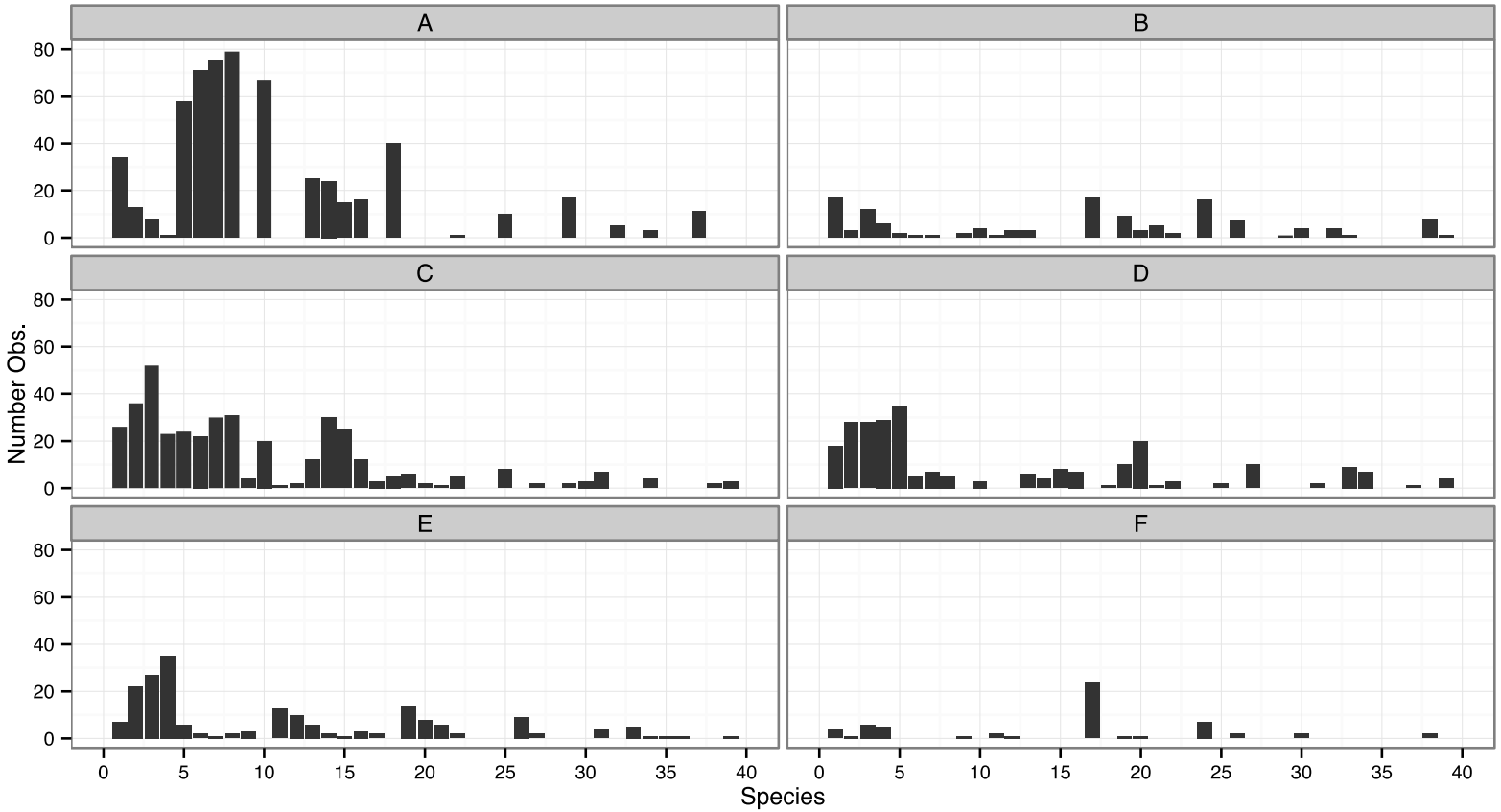

Figure D.3. The number of observations of each species faceted by vegetation association cluster assignment. Relate species number to species name using Table A.1.

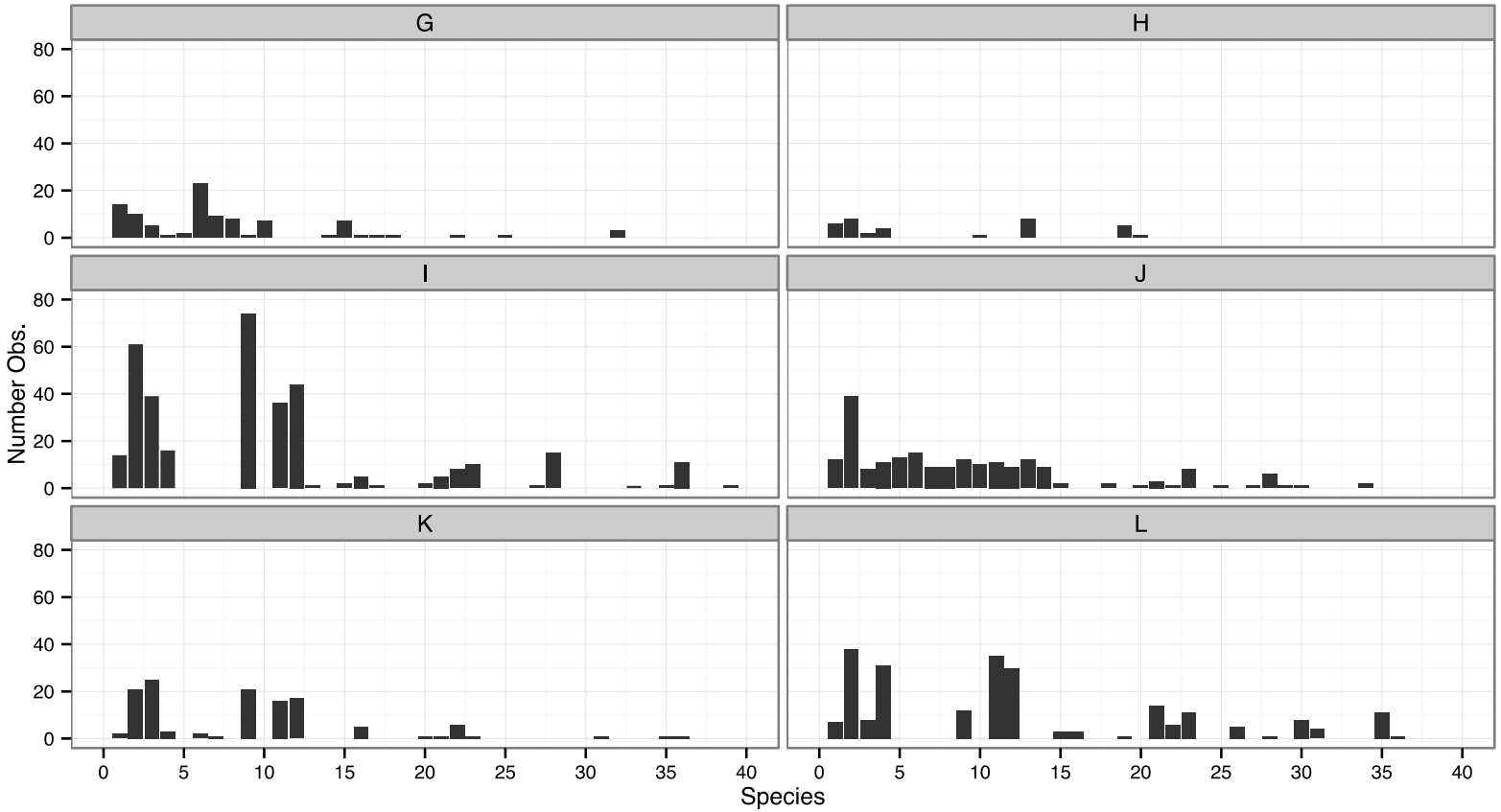

Figure D.3 (continued). The number of observations of each species faceted by vegetation association cluster assignment. Relate species number to species name using Table A.1.

APPENDIX E

Non-metric Dimensional Scaling

APPENDIX E NON-METRIC DIMENSIONAL SCALING

Non-metric dimensional scaling (NMDS) is a multivariate technique to visualize high dimensional data. We used NMDS to visualize the difference between datapoints and clusters within my 40-dimensional vegetation composition hyperspace. In addition, we fit gradients to the NMDS ordination. These fits were weak ($r^2 < 0.10$), but may still provide context to the vegetation association clusters (Figure E.2, Table E.1, Chapter 3). NMDS was performed using the package *vegan* (version 2.0-7; Oksanen *et al.*, 2013). A convergent NMDS solution was not found after 50000 iterations. The final stress after 50000 iterations was 0.174, on the upper limit of acceptable based on the recommendations provided within McCune *et al.* (2002).

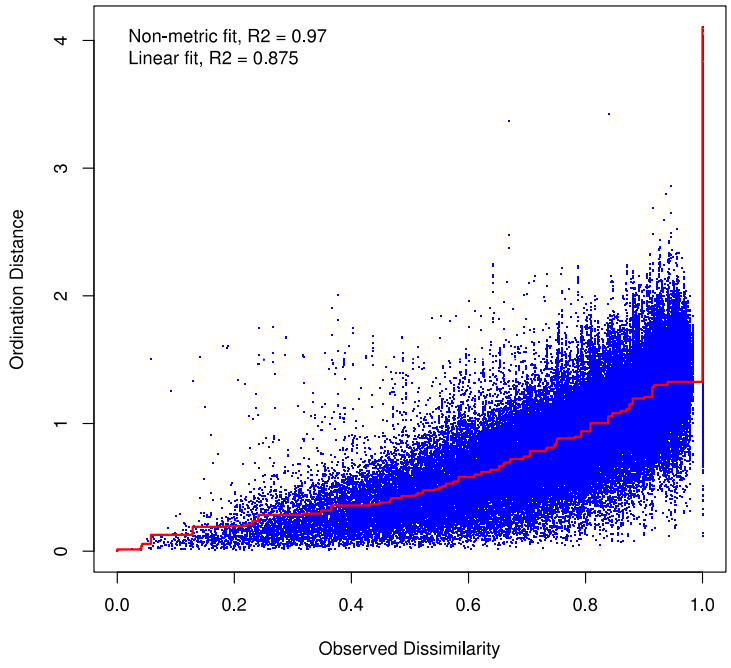

Figure E.1. NMDS stress plot

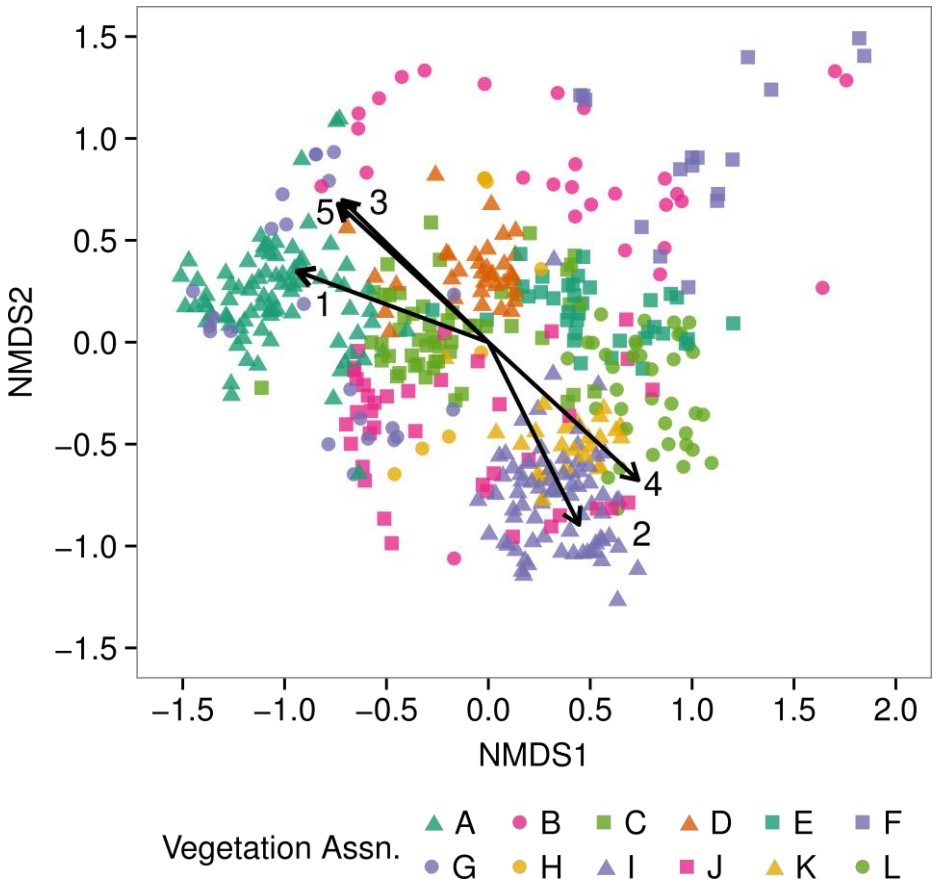

Figure E.2. NMDS plot of vegetation data. Data points are colored by vegetation association. Data points are colored by vegetation association, with gradients fit to the ordination space. Relate the NMDS vector to its gradient using Table E.1.

Table E.1. NMDS Gradients

	NMDS Gradient	NMDS1	NMDS2	R2	p-value
1	NAVD88 Elevation	-0.9377	0.3475	0.051	< 0.001
2	LIDAR Point Density (all returns)	0.4450	-0.8955	0.020	0.009
3	Std. Dev. LIDAR Intensity (all returns)	-0.7166	0.6975	0.082	< 0.001
4	Total Plant percent cover	0.7361	- 0.6768	0.022	0.007
5	Bare-ground percent cover	-0.7360	0.6770	0.022	0.006

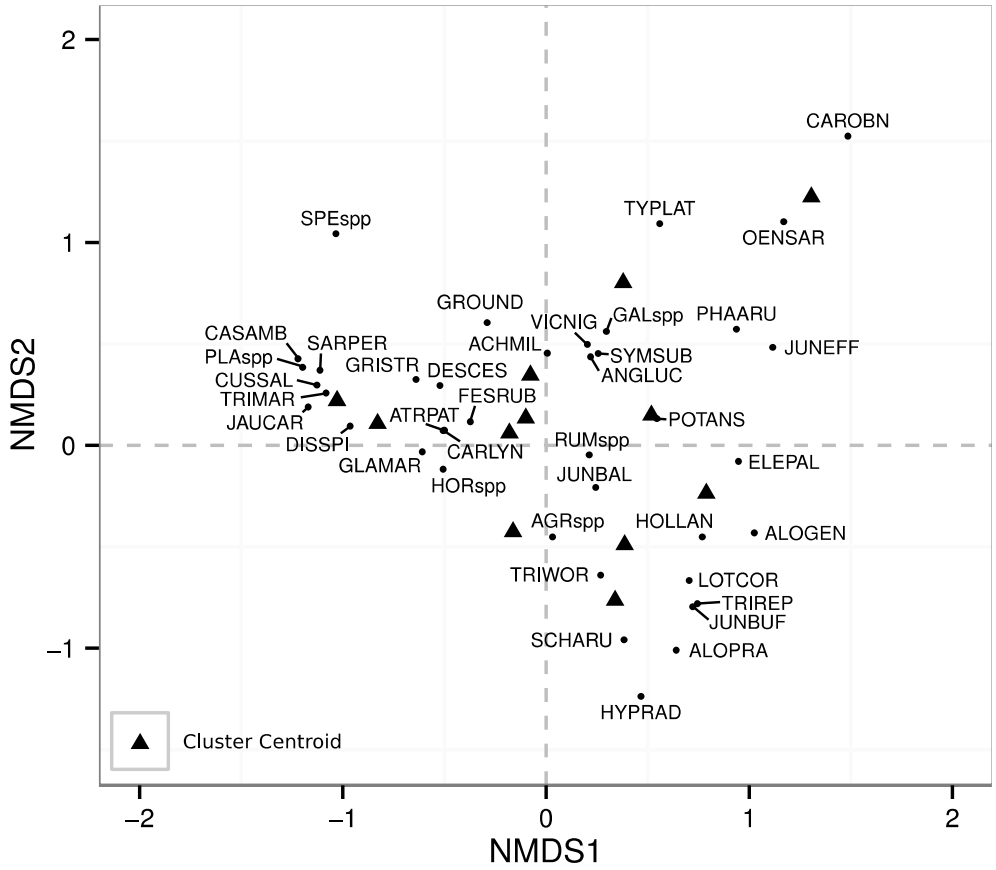

Figure E.3. Species centroids within the NMDS ordination space. Each black triangle represents the cluster centroid (also shown in Figure E.2). Solid circles represent the species centroid. Refer to Table A.1 to associate six-letter species codes to each species.

APPENDIX F

Vegetation Association Cluster Diagnostic Plotting

APPENDIX F VEGETATION ASSOCIATION CLUSTER DIAGNOSTIC PLOTTING

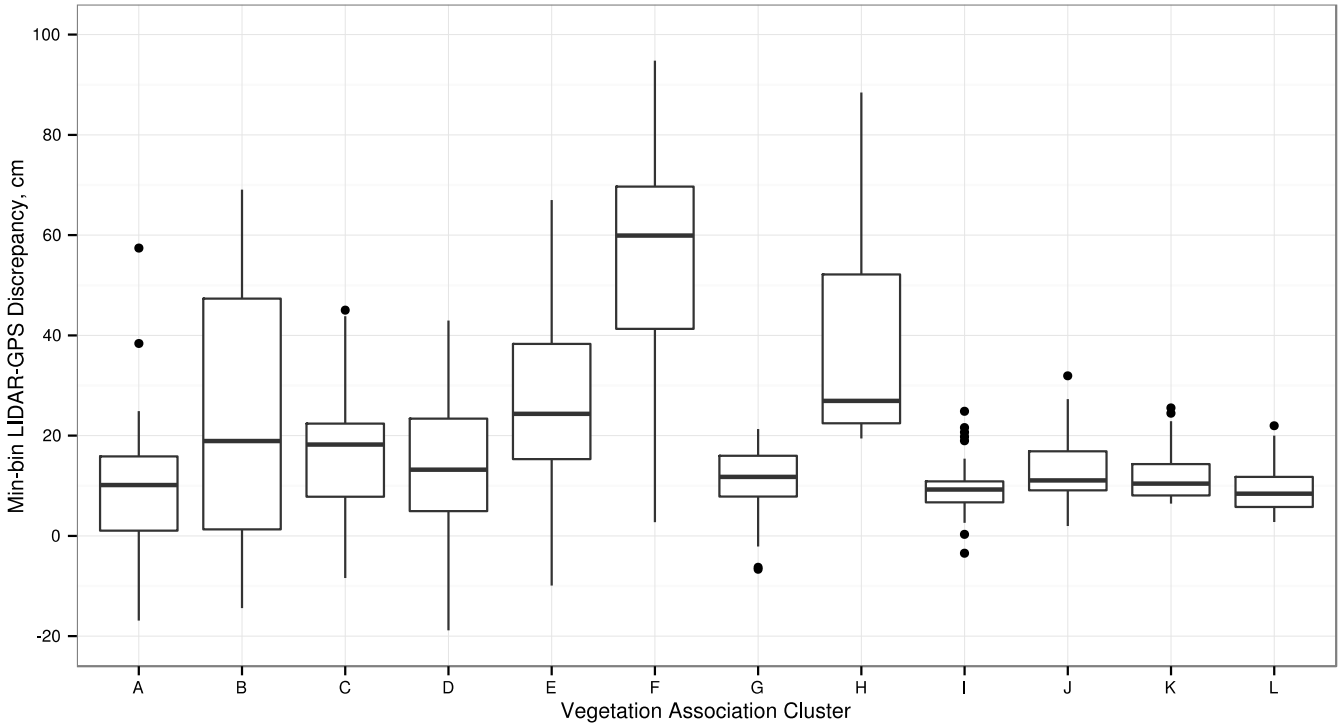

Figure F.1. Minimum-bin LIDAR-GPS discrepancy boxplot by vegetation association cluster

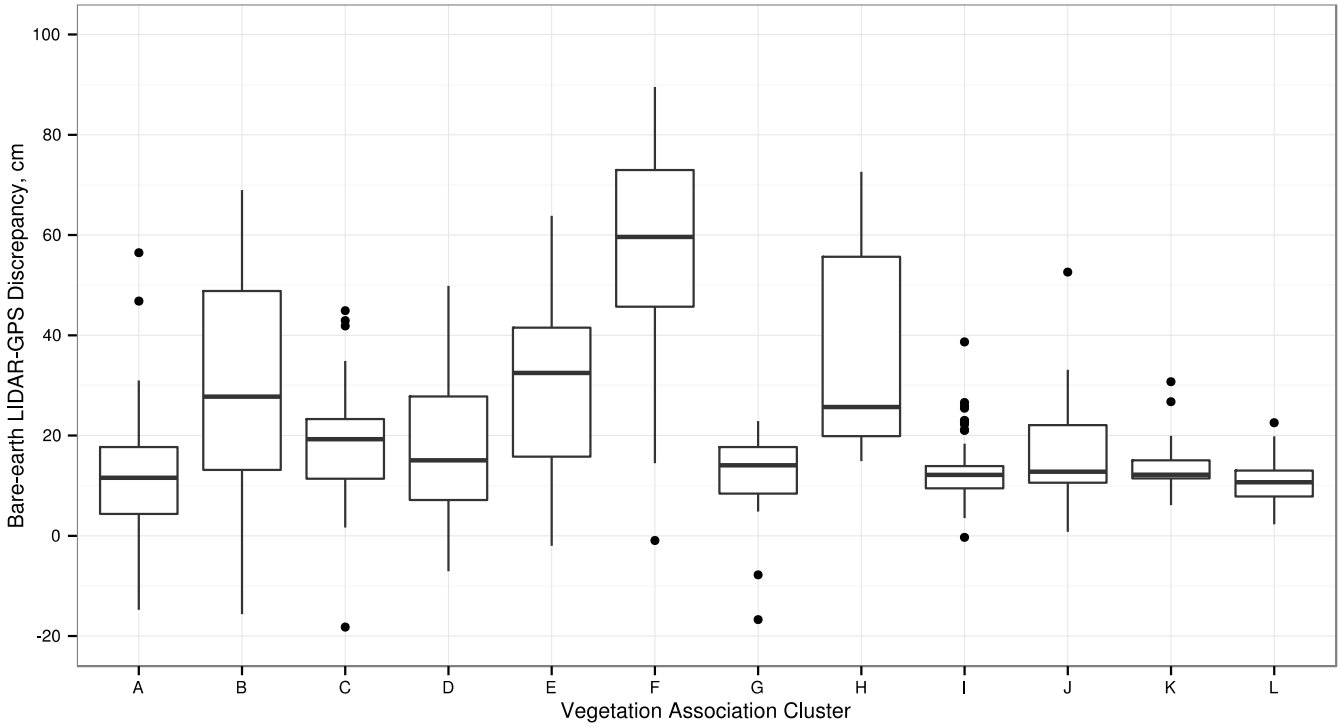

Figure F.2. DOGAMI bare-earth LIDAR-GPS discrepancy boxplot by vegetation association cluster

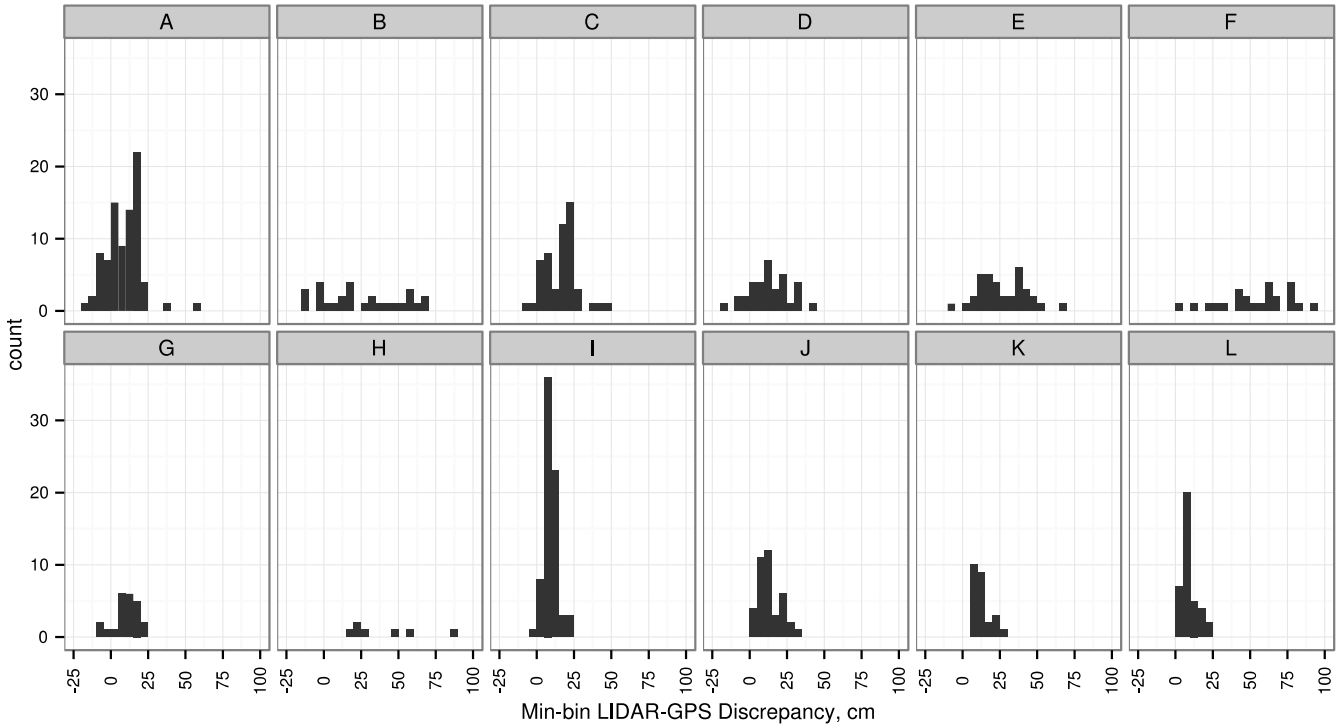

Figure F.3. Minimum-bin LIDAR-GPS discrepancy histogram plots faceted by vegetation association cluster. Table A.1 relates species number to species name.

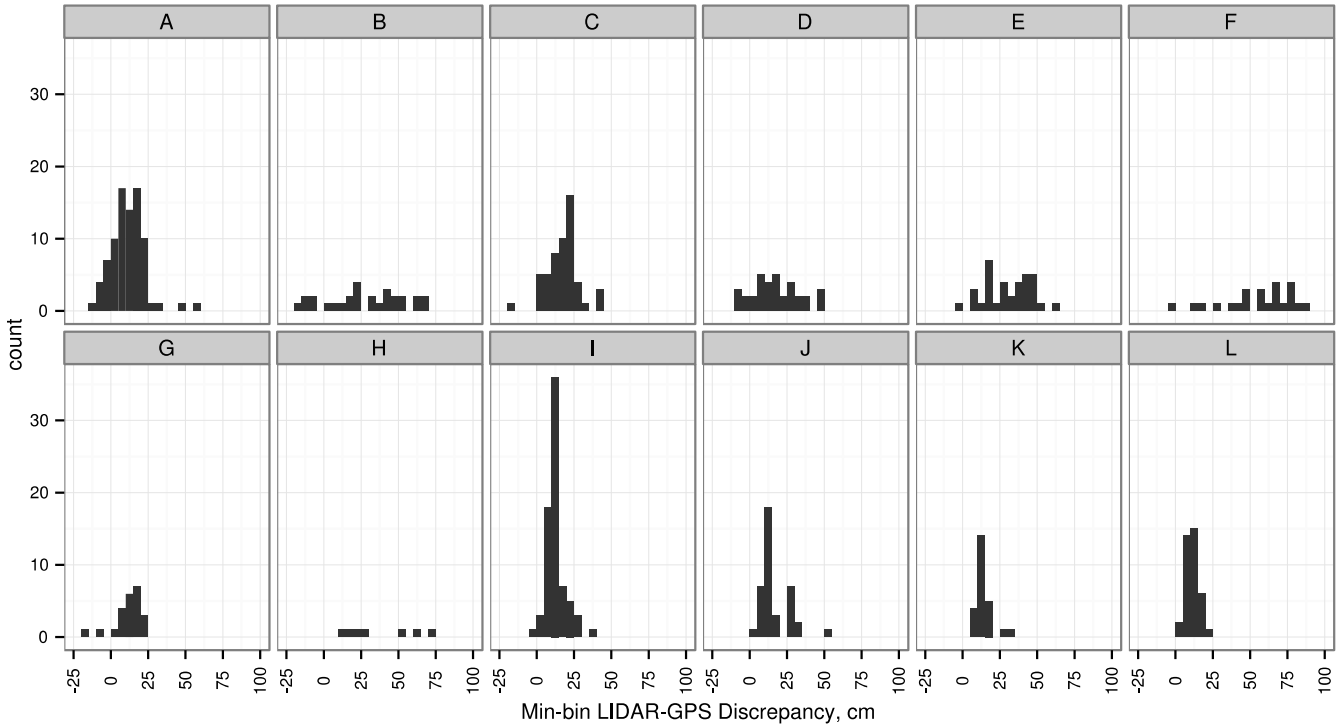

Figure F.4. DOGAMI bare-earth LIDAR-GPS discrepancy histograms faceted by vegetation association cluster. Table A.1 relates species number to species name.

APPENDIX G

Mixed Effect Model Validation Plots

APPENDIX G MIXED-EFFECT MODEL VALIDATION PLOTS

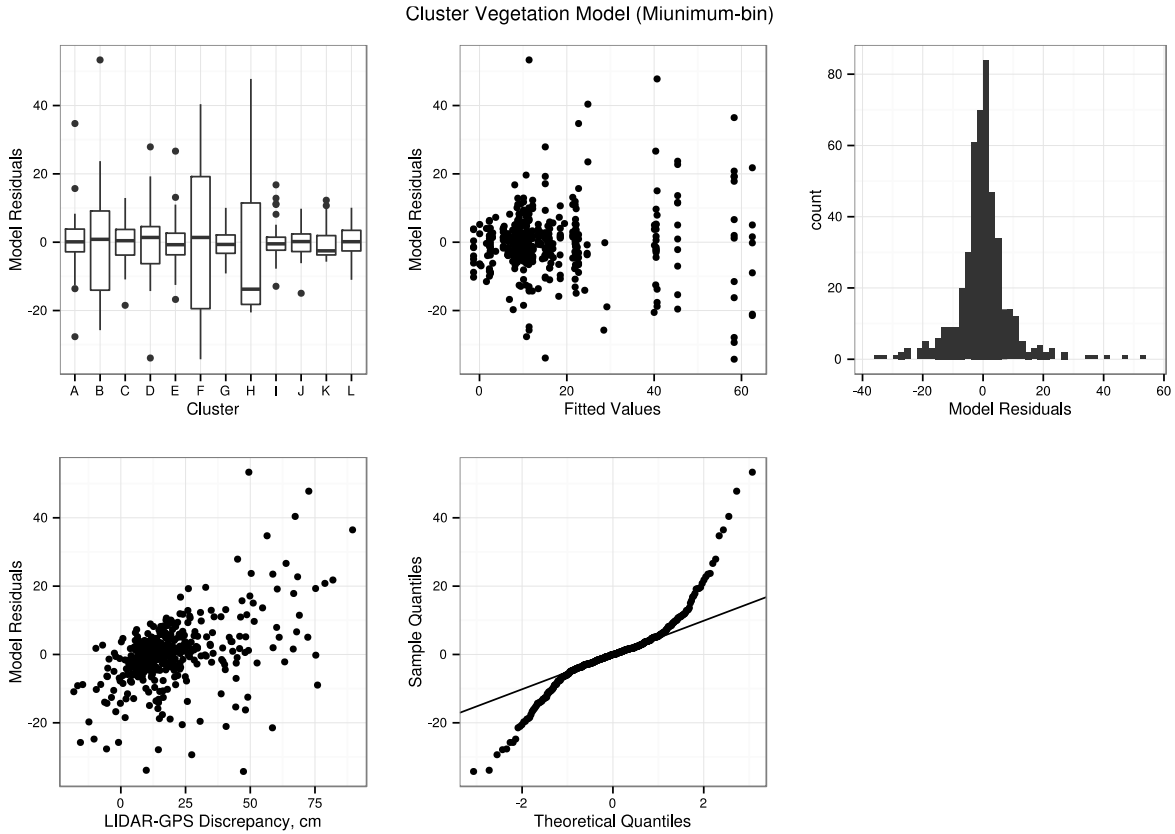

Figure G.1. Minimum-bin LIDAR-GPS mixed model validation plots

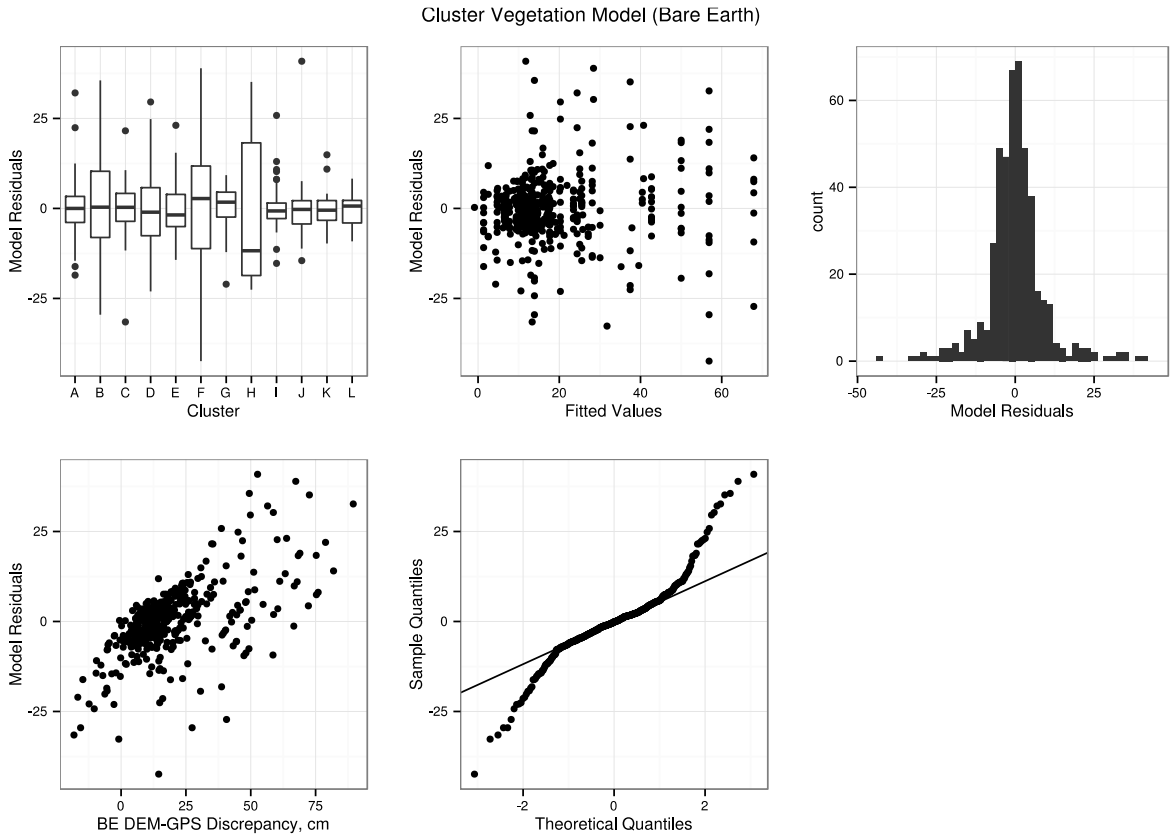

Figure G.2. DOGAMI bare-earth LIDAR-GPS mixed-model validation plots

APPENDIX H

Spatial Reference

APPENDIX H SPATIAL REFERENCE

H.1 Horizontal Coordinate System

Name	Oregon Statewide Lambert
Projection	Lambert Conformal Conic
Datum	North American Datum of 1983 (NAD83) - CORS96 - Epoch 2002
Spheroid	Geodetic Reference System 1980 (GRS80)
Units	International Feet (0.3048 m exactly)
EPSG Code	2992
1st Standard Parallel	43.0 degrees
2nd Standard Parallel	45.5 degrees
Central Meridian	-120.5 degrees
Latitude of Projection's Origin	41.75 degrees
False Easting	1312335.958 Intl. Ft.
False Northing	0.000 Intl. Ft.

H.2 Vertical Datum

Datum	North American Vertical Datum of 1983 (NAVD83)
Units	Meters
Geoid Model	GEOID03